CHAPTER 4 RESULTS AND DISCUSSION

4.1 Introduction

This chapter presents the results of analyses of the problem of rock masses surrounding a high pressure gas storage cavern. It consists of three parts which are the evaluation of crack initiation, preliminary evaluation on failure patterns and failure mode of fracture propagation. The description in this section is discussed about the corresponding overall results of each part to the others.

The results of the crack initiation and the preliminary evaluation are performed with the stress analysis by using ABAQUS program, through a wide range of parameters including in-situ stress ratio and strengths of rock masses. As a result, it was found a crucial point having an interest for the failure behaviors in rock masses around the pressurized gas storage cavern. That is the concept of the line of D/R=1. Based on the concept of this line, when the relationship between tensile strength and cohesion locates above this line, it implies that tensile failure reaches its criterion. While these relationship are situated under the line of D/R=1, shear criterion is yielded.

One of the objectives of this research is to study the fracture propagation behaviors of rock masses surrounding a high pressure gas storage cavern considering both tensile and shear failure. With the crucial found in the crack initiation and the preliminary evaluation section is the concept of the line of D/R=1. In order to achieve the goal of this study and validate the concept of the line of D/R=1, some carefully selected cases are to be analyzed in progressive failure analysis in conjunction with contact-friction interface by using ABQUS program with its special subroutine. The case selection is exploited from the consideration of the wide range of rock properties obtained from those stress analysis parts.

The progressive failure analysis starts with pre-determination of three potential failure paths considering on both tensile and shear planes. Along those failure paths, the contact-friction interface is modelled. The interface with a special algorithm governed by Coulomb and tensile failure criteria has been developed and written for this study. Once along those failure paths, the crack will be propagated when stress states reached one of the failure criteria. The results of progressive failure analysis are then to be observed. Moreover, there is also the verification case with the previous study by Tunsakul et al. (2013) to prove the concept of the line of D/R=1.

4.2 Evaluation of crack initiation

The failure behavior in terms of position of crack initiation and corresponding failure modes are described. It is noted that all analysis cases have been conducted until the stress reaches to the critical value of which the failure criterion is satisfied.

In this study, the parameters to be investigated their effect on crack initiation in this part include the depth, in-situ stress ratio *(k)* and strength of rock mass. To represent the actual field, in-situ geostatic stress conditions are applied in the analyses.

4.2.1 Observation of stress states with crack initiation criteria during applying the cavern pressure

The increasing of the cavern pressure results to the gradual increase of the major principal stresses (σ_1) (compression: negative) at the cavern periphery (decrease in compression and then change from compression to tension). On the other hand the minor principal stress (σ_3) decreases (gradually increase in compression). With consideration of both tensile and shear criteria, the location that yields the maximum principal stress (σ_1) indicates the failure initiation location for the tensile failure mode. For shear failure consideration, by increasing the cavern pressure, the values of D/R gradually reduce until the location at which minimum D/R equals to 1, is indicated for the shear failure initiation location. From wide range of rock strength properties, the values of tensile strength (σ_t) and cohesion (C) are in the range of 2 – 35 and 3 – 60 MPa, respectively. The tensile failure criterion of rock mass depends on the tensile strength (σ_t) while the frictional angle ($\varnothing$) and cohesion (C) represent for shear failure criterion.

In Figure 4.1, the example results of analysis of cavern with depth of 60 m and k of 1 is presented. The Figure shows the evolution of maximum σ_1 and D/R with increasing cavern pressure to 10, 15 and 20 MPa. For tensile failure consideration, the values of the maximum σ_1 which are induced from the cavern pressure increase to 3.01, 5.80, and 8.60 MPa, respectively. By strictly setting shear criterion with the value C of 10 MPa and $\varnothing$ of 45° ($\varnothing$ is constant of 45 in this research), the minimum D/R decreases to 1.4, 1 and 0.78 with increasing the cavern pressure of 10, 15 and 20 MPa, respectively.

Figure 4.2 shows the stress states considered on Mohr-circle of this example result. By varying the values of tensile strength (σ_t) for tensile criterion, there are three situations for considering of failure mode on crack initiation which is obtained from this example. First situation, at the cavern pressure of 10 MPa, the minimum σ_3 reaches tensile failure criterion if tensile strength (σ_t) is 3.01 MPa and the tensile failure is only specified. Second, if tensile strength (σ_t) is 5.80 MPa, both tensile and shear failure criteria are satisfied at the same time. This situation occurs at 10 MPa of the cavern pressure. Third situation, at the cavern pressure of 20 MPa, if tensile strength (σ_t) is 8.60 MPa shear failure is only determined because shear failure has been occurred at 15 MPa of the cavern pressure. This implies that with the shear strength parameters C and $\varnothing$ of 10 MPa and 45°, the tensile failure will occur if the tensile strength (σ_t) of rock is less than 5.80 MPa. With the tensile strength (σ_t) larger than this value, shear failure mode will occur. Therefore, either tension or shear failure mode can occur in rock mass around the pressurized cavern depending on the strength properties of rock which are the relationship between tensile strength (σ_t) and cohesion (C) (the other shear strength variable, $\varnothing$, is controlled to be 45° in this research).

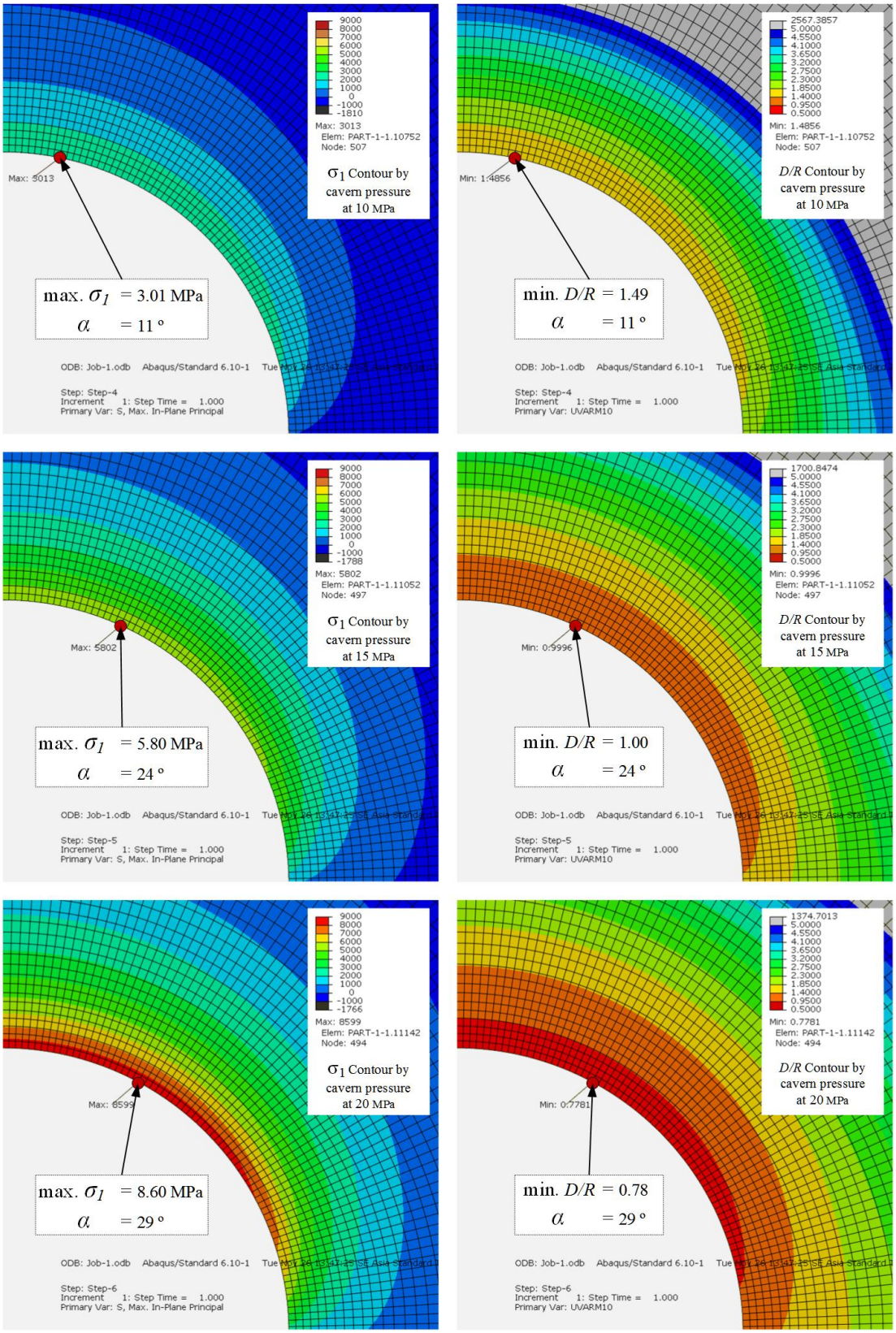

(a) Tensile failure initiation (b) Shear failure initiation

Figure 4.1 The example of the crack initiation of both shear and tensile modes during applying the cavern pressure of 10, 15 and 20 MPa with *k* of 1 and depth of cavern of 60 meters

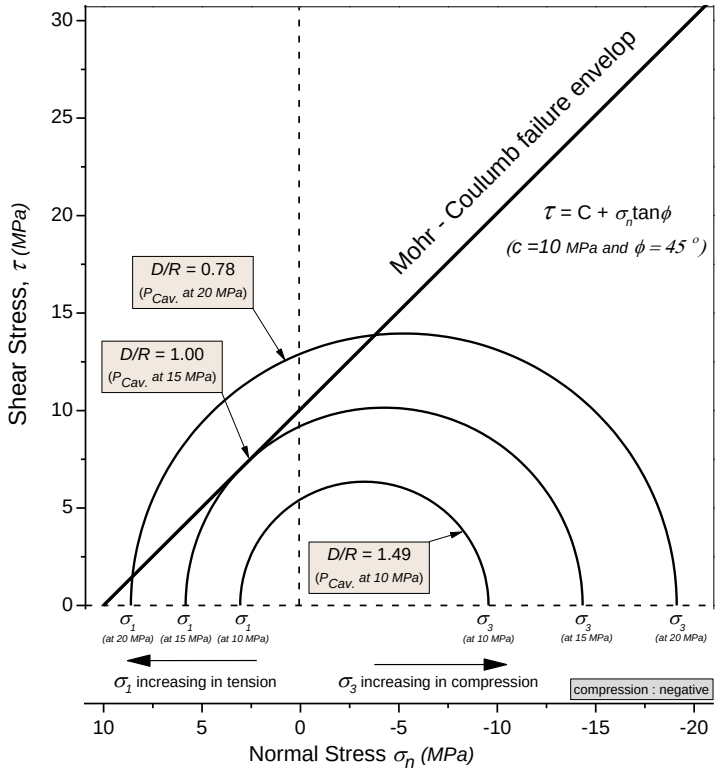

Figure 4.2 The stress states considered as Mohr circles

In addition, the locations that indicated the initial failure of both failure modes are also described in this section. In this study, the location is presented as failure angle which is defined as shown in Figure 4.3.

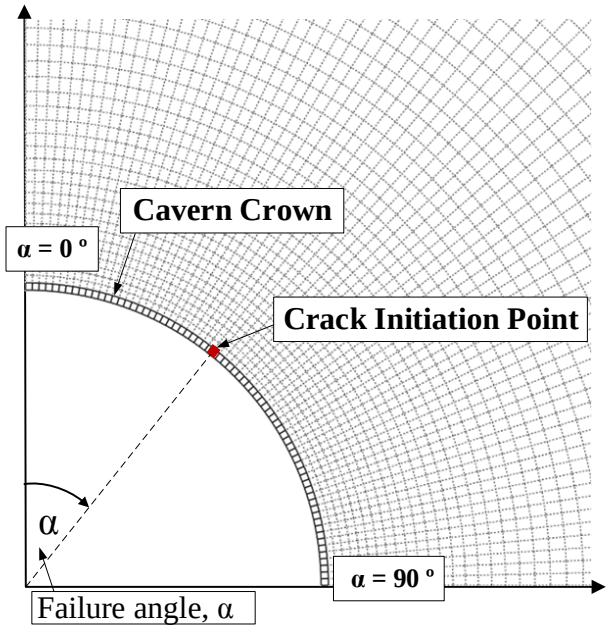

Figure 4.3 Definition of failure angle (α) for crack initiation point

From the Figure 4.1, at each different level of applied cavern pressure, it is clearly seen that the locations of both failure modes are the same. In the example case in Figure 4.1; the cavern depth and *k* of 60 m and 1, the locations of crack initiation are 11, 24, 29 degrees (°) at the cavern pressure of 10, 15, 20 MPa, respectively. Thus, the transition of the location of crack initiation can be seen. This implies that, with different strengths of rock, the location of crack initiation can be altered. This is because the internal pressure required for crack initiation becomes different.

As described above, with increasing the cavern pressure, the values of the maximum σ_1, the minimum *D/R* and failure angle in each analysis case are collected in calculation data. Table 4.1 shows the example of the calculation data in case of the cavern depth and *k* of 60 m and 1. From Figure 4.1, as highlighted in grey, the values are collected in this table with level of applied cavern pressure of 10, 15, 20 MPa. By setting shear criterion with varying 5 MPa increment in cohesion, the calculation data are obtained.

Table 4.1 The example of calculation data in case of the cavern depth of 60 meters and *k* of 1

P. cav (MPa)	Max of σ_1 (MPa)	Minimum of D/R with varying cohesion (MPa)					Failure angle (degrees, °)
		5	10	15	20	25	
5	0.23	2.03	3.41	4.80	6.19	7.57	4
10	3.01	0.93	1.49	2.04	2.60	3.16	11
15	5.80	0.65	***1.00***	1.35	1.70	2.04	24
20	8.60	0.52	0.78	***1.03***	1.28	1.54	29
25	11.40	0.45	0.65	0.85	***1.05***	1.25	30

From the information as listed in Table 4.1, the pair of σ_1 (represents for tensile strength) and *C* of which yields the D/R of 1 represents the case that both failure criterion are simultaneously satisfied. With the tensile strength lower than this σ_1, tensile failure dominates. On the other hand, the failure would be governed by shear mode if the tensile strength becomes larger than this σ_1. The line of this relationship (line of many pairs) can be used as the boundary to distinguish between the shear and tensile failure.

With varying 5 MPa increment of the cohesion in the analysis, in order to create the line, it is necessary to select the values of D/R which is close to 1. The range of D/R of 0.95 - 1.05 are used in this study and the line is obtained by linear regression.

Figure 4.4 shows the results of linear regression in case of the cavern depth and *k* of 60 m and 1 obtained from the entire calculation data. The values in the calculation data which is in the range of D/R of 0.95 - 1.05 are plotted. It is noted that three data points as shown with italic marked text in Table 4.1 were also included in this Figure.

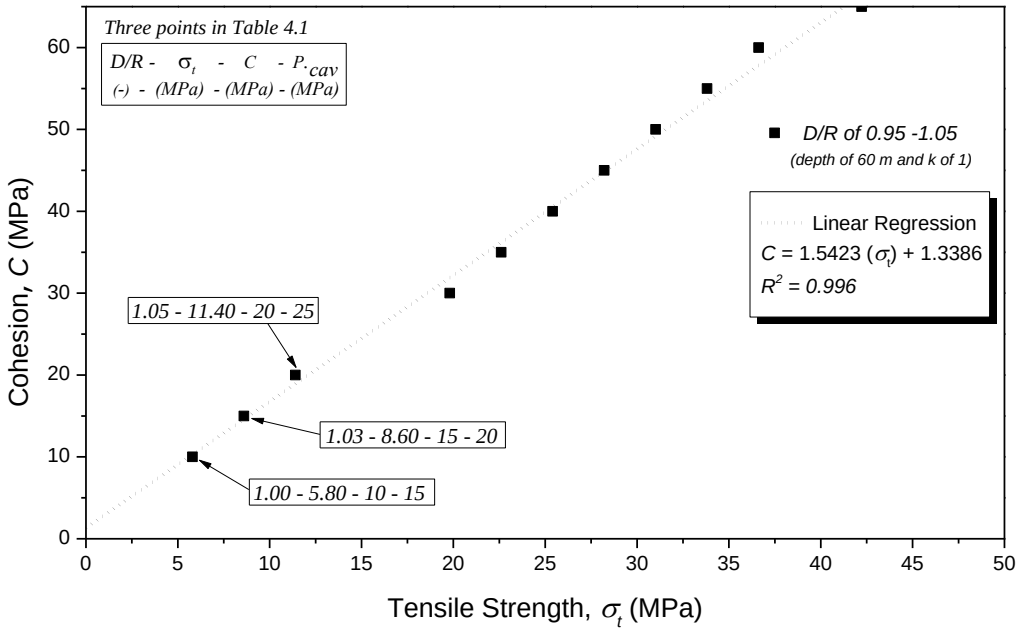

Figure 4.4 Linear regressions for line of D/R=1 in case of the cavern depth of 60 meters and *k* of 1

It is seen that the transition of the location of crack initiation can be occurred as aforementioned shown in Figure 4.1. Figure 4.5 shows the relationship between possible failure angles against rock strength by plotting all data in case of the cavern depth and *k* of 60 m and 1. It is noted that there are also five points as shown in Table 4.1 which is illustrated in this Figure. Moreover, the effects of some factors on initial crack location will be described in following in section 4.2.3.

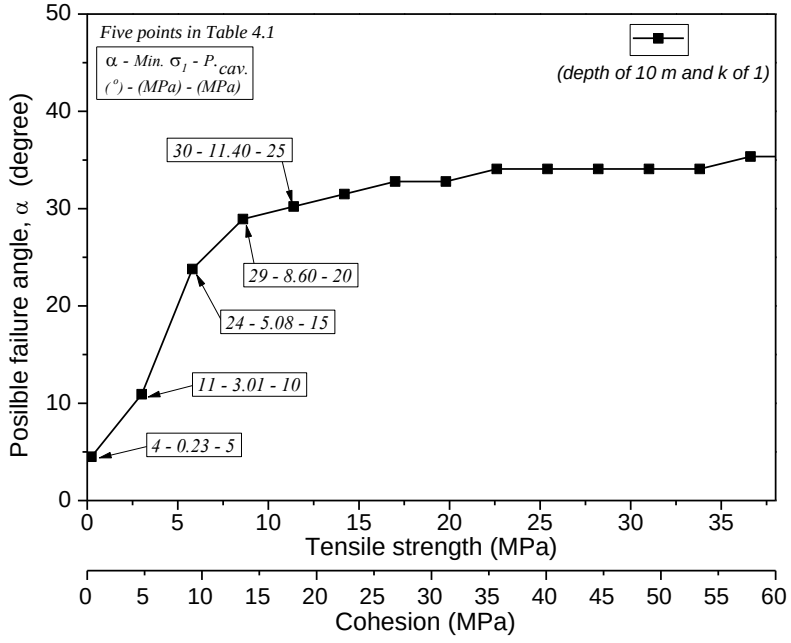

Figure 4.5 The transition of the location of crack initiation in case of the cavern depth and *k* of 60 m and 1

From the overall data for all cases, the results can be altogether plotted as shown in Figure 4.6 The linear regression method is adopted to find the relationship between the cohesion and tensile strength values at which both failure modes simultaneously initiate for the data of all cases (various depths and *k* values as listed in Table 3.3) as shown in Figure 4.6.

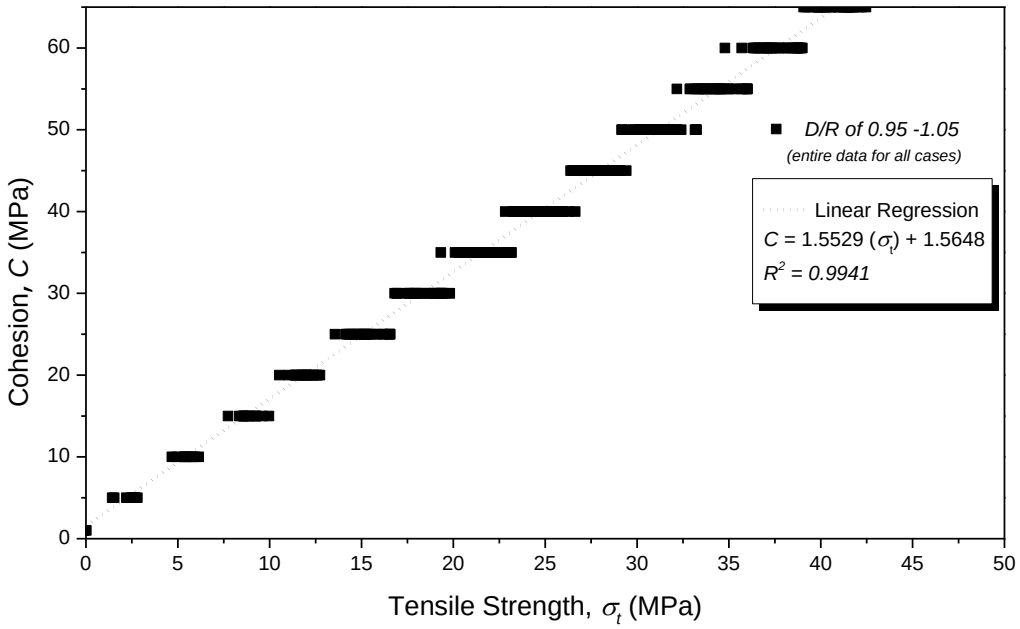

Figure 4.6 Line of D/R=1 obtained from all cases

4.2.2 Effect of influencing parameters on crack initiation point

The parameters to be investigated their effect on crack initiation point in this part include the depth, in-situ stress ratio *(k)* and the strengths of rock mass (tensile strength: 2-35 MPa and cohesion: 3-60 MPa).

Figure 4.7 shows the relationship between the possible failure angle (crack initiation point with respect to cavern crown) against the tensile strength of rock mass during applied internal pressure for cavern depths of 60, 80, 100 and 150m.

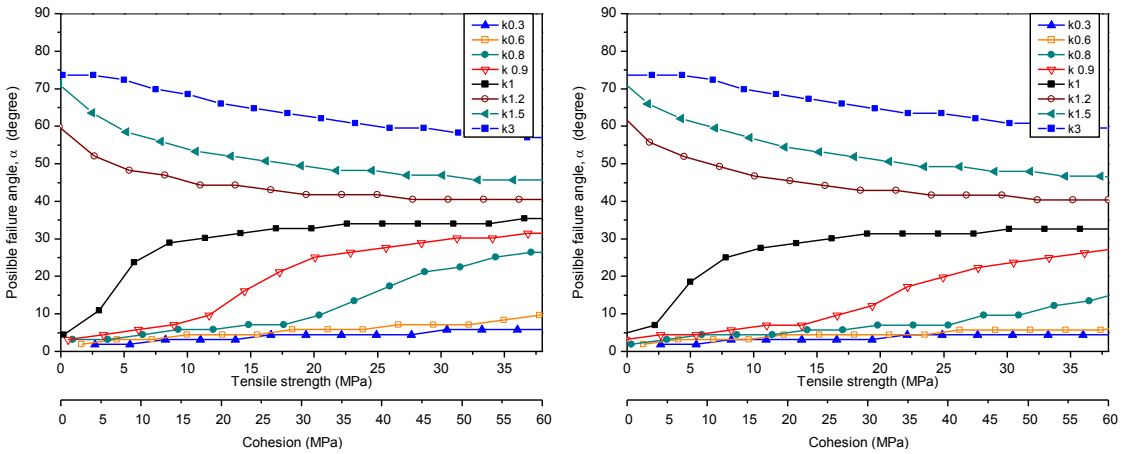

Depth 60 m Depth 80 m

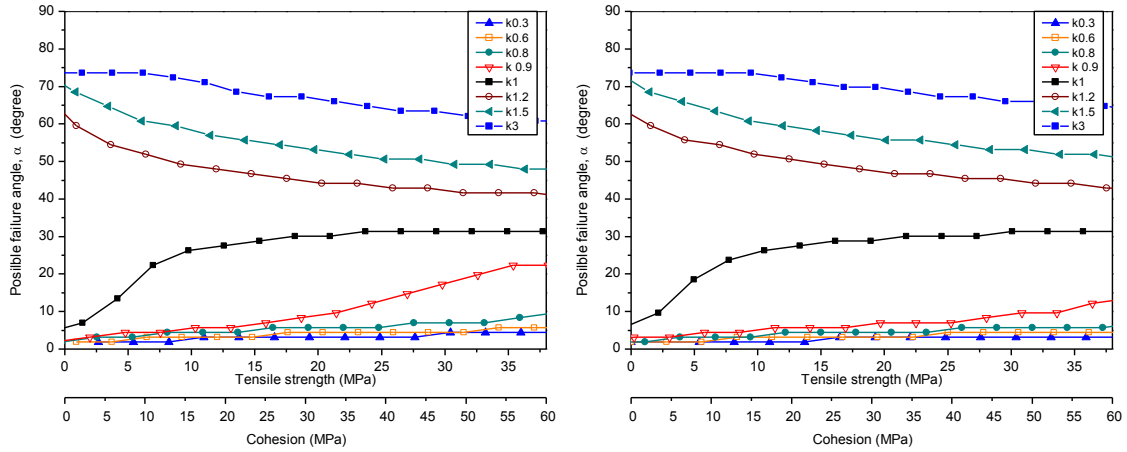

Depth 100 m Depth 150 m

Figure 4.7 Influence of tensile strength on the possible failure angles for various cavern depths

From the observation, it can be seen that, for cases of k <1, the possible failure angles are found at around the cavern roof. For k of 0.3 and 0.6, with all tensile strength values in the range of this study, the failure initiation point is always at cavern crown (α = 4°). With increasing tensile strength and k, the location moves from the cavern crown to the roof with angle of approximate 35°.

The transition of failure initiation point (from roof to failure angle of 35°) still depends on the depth at which the cavern is located. With increasing depth, the failure initiation point tends to be at cavern crown. In contrast, for cases of k >1, the results reveal that the locations of failure initiation mostly appeared at the cavern wall ($\alpha \geq$ 45°). With increasing tensile strength and deceasing k, the location moves from the cavern wall to the roof with angle of approximate 45°.

However, with high value of k (larger than 1.5), the crack initiation point is always at the wall with $\alpha \geq$ 45° regardless of the depth and tensile strength of rock mass.

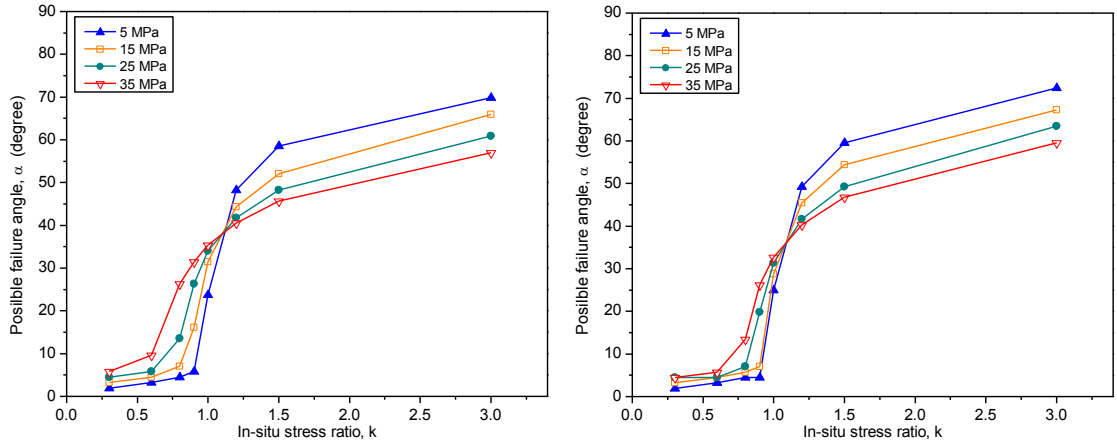

Depth 60 m Depth 80 m

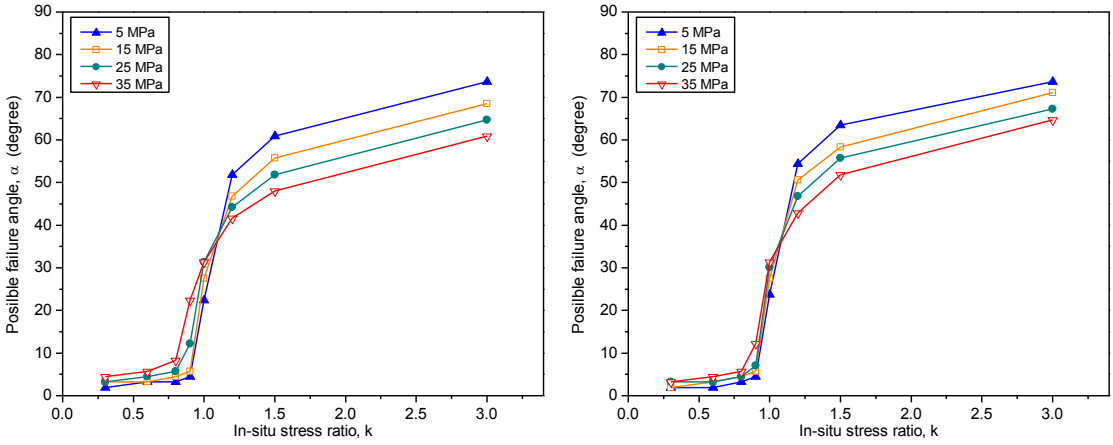

Figure 4.8 Influence of in-situ stress ratio on the possible failure angles for various cavern depths

To clearly investigate the influence of *k* on the possible failure angle, the possible failure angles are re-plotted with *k* as shown in Figure 4.8. All results for various depths indicate that the *k* has strong influence on the possible failure angle.

The same patterns of the locations of the possible failure angles are also found for each tensile strength and depth. The possible failure initiation points along the cavern periphery move from the cavern crown to the cavern wall with increasing *k*. The sudden transition of the possible failure angles at cavern crown to wall, approximately, from 4° to 35° occurs at *k* in the range of 0.8 to 1.

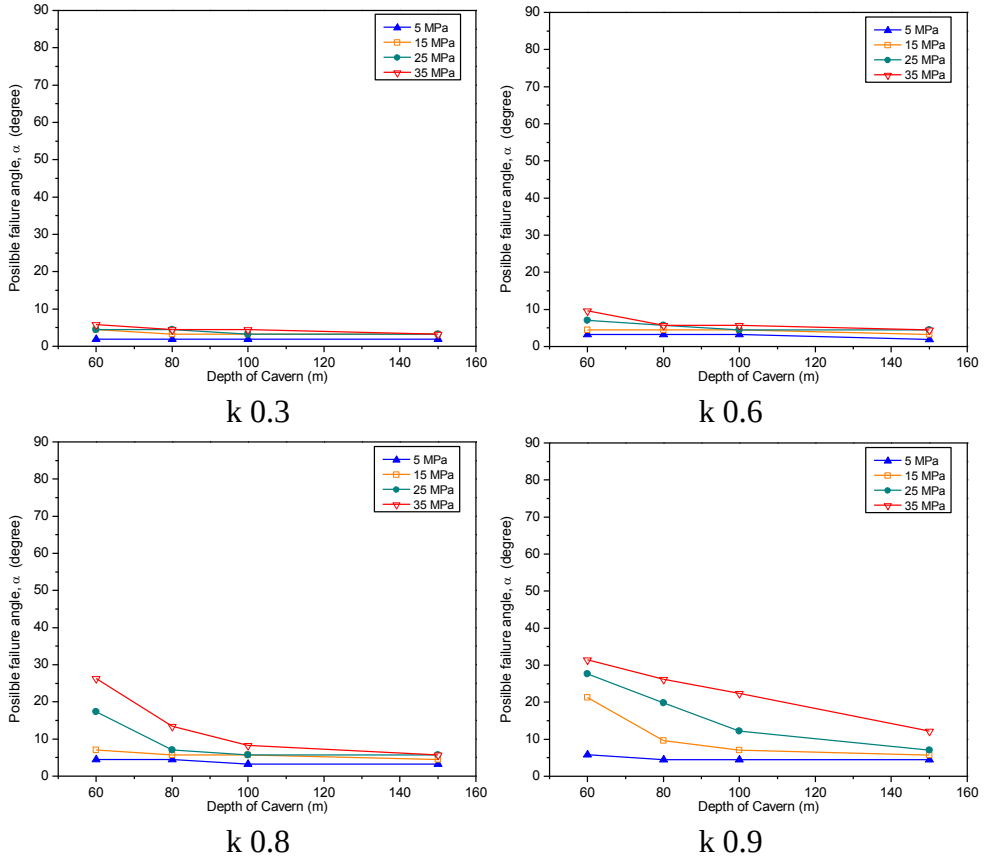

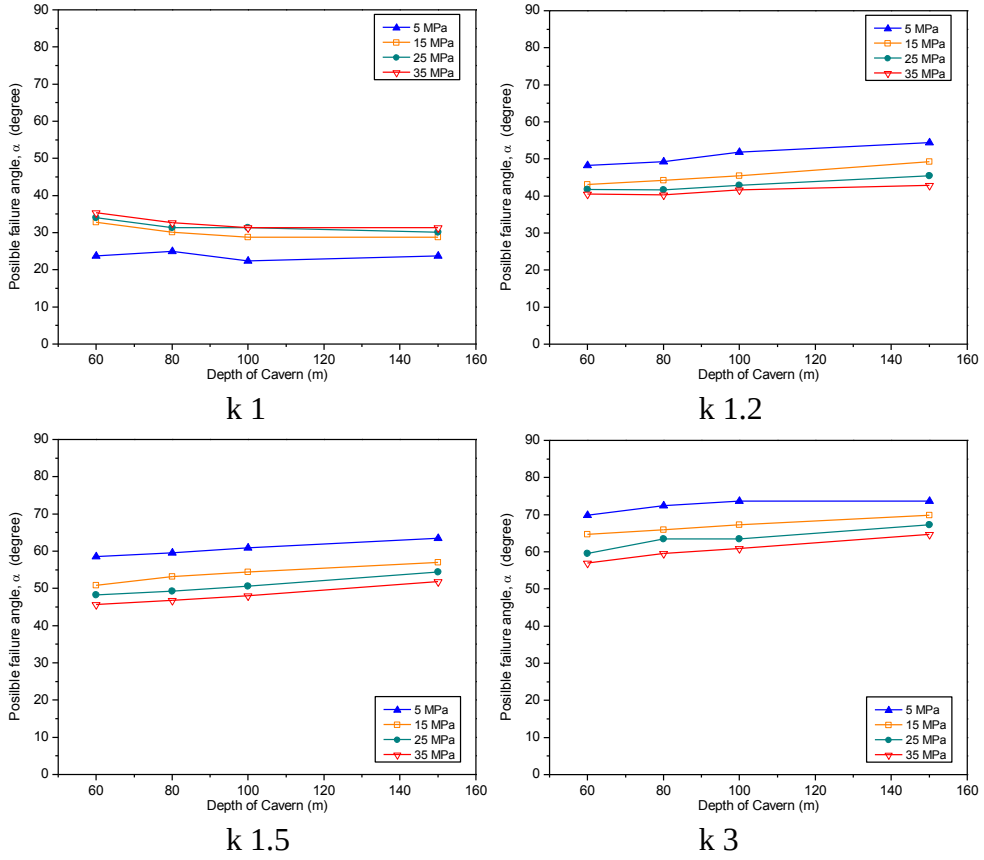

Figure 4.9 Influence of depth of cavern on the possible failure angles for various in-situ stress ratio

Figure 4.9 shows the influence of depth on the possible failure angles for various *k* values. From the observation, the tendency can be divided into 3 groups depending on the range of *k*.

For the first group, with k = 0.3 and 0.6, the depth and tensile strength of rock mass have insignificant influence on the possible failure angles. The failure initiation always happens at cavern crown with failure angle of 4° regardless of tensile strength of rock or cavern depth in the ranges of study. The possible failure angles of the second group exhibit decreasing trend of failure angle (from about 35°or less to 4°) with increasing depth, meaning that the failure initiation point move from the cavern crown with angle approximately 35 ° to cavern crown approximately 4°. This happens when the k is in the range of 0.8 to 0.9. In the same manner, with k = 1, the possible failure angles also exhibit slightly decreasing trend with the increasing depth, and the possible failure angles distinctly move to cavern crown with the angle of 4° especially in case of tensile strength = 5 MPa. In contrast, for range of k from 1.2 to 3, the possible failure angle slightly increases while the depth increases. At the same depth and tensile strength, the increasing value of failure angle occurs when the value of k is increasing. In addition, the larger values of failure angle happen with lower tensile strength.

4.2.3 Conclusion

From the analysis results, there are 2 points to be concluded.

First, by considering the boundaries of typical rock strengths as described in section 3.2, the line of D/R=1 is proposed in this study to assist evaluation of the failure mode for crack initiation. The line of D/R=1 refers to the relationship between the tensile strength and cohesion of rock of which the tensile and shear failures would simultaneously occur. The line is embedded in the boundaries of typical rock strengths, becoming a chart to distinguish the failure mode in this study as shown in Figure 4.10. From Figure 4.10, when the relationship of σ_t and C which are situated above the *line of D/R*=1, the tensile mode is expected to act on fracture behavior. In contrast, if the relationship is located under this line, shear fracture behavior is to be anticipated. It is noted that the expectation of two fracture behaviors as discussed in this section will be further analyzed in section 4.3.

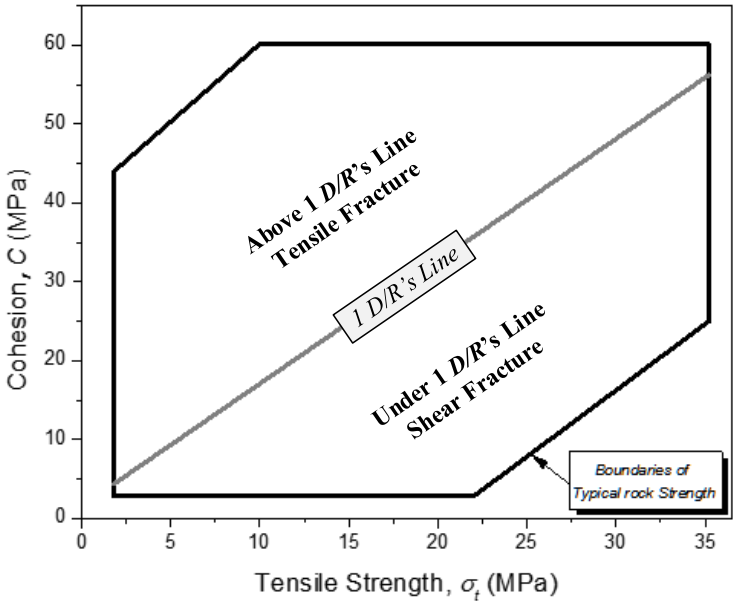

Figure 4.10 Chart to determine the failure mode

Second, the transition behavior of crack initiation location, as described in section 4.2.2 is discussed. This behavior depends mainly on two significant factors which are *k* and rock strength, while the depth of cavern becomes insignificant factor.

The results from section 4.2.2 could be illustrated in a new format in order to clearly investigate the other influencing factors. By this format, two significant factors are more noticeable for their influence on the transition behaviors of crack initiation location. In the new format, the failure angle (α) is represented by the radial lines with 5º increments of the angle in the quarter circle (quadrant I) as shown in Figure 4.11. It is seen that the radial lines is mentioned the similarity of the initial crack location for failure angle.

In terms of the transition of the initial crack location, the circumferences with different radius distances are used to represent and indicate the initial crack location in each value of *k*. In addition, the tensile strength (σ_t) in the different values of 2, 15, 25 and 35 MPa are presented by four line segments intersecting with the circumferences having different *k* values. From the behaviors of initial crack location as discussed in section 4.2.2, when $k \leq 1$ the initial locations are situated in the range of failure angle of 2 –

35°, while the range of failure angle of 40 – 75° is appeared when $k > 1$. Noted that, the depth of cavern has insignificant effect of the transition initial crack location

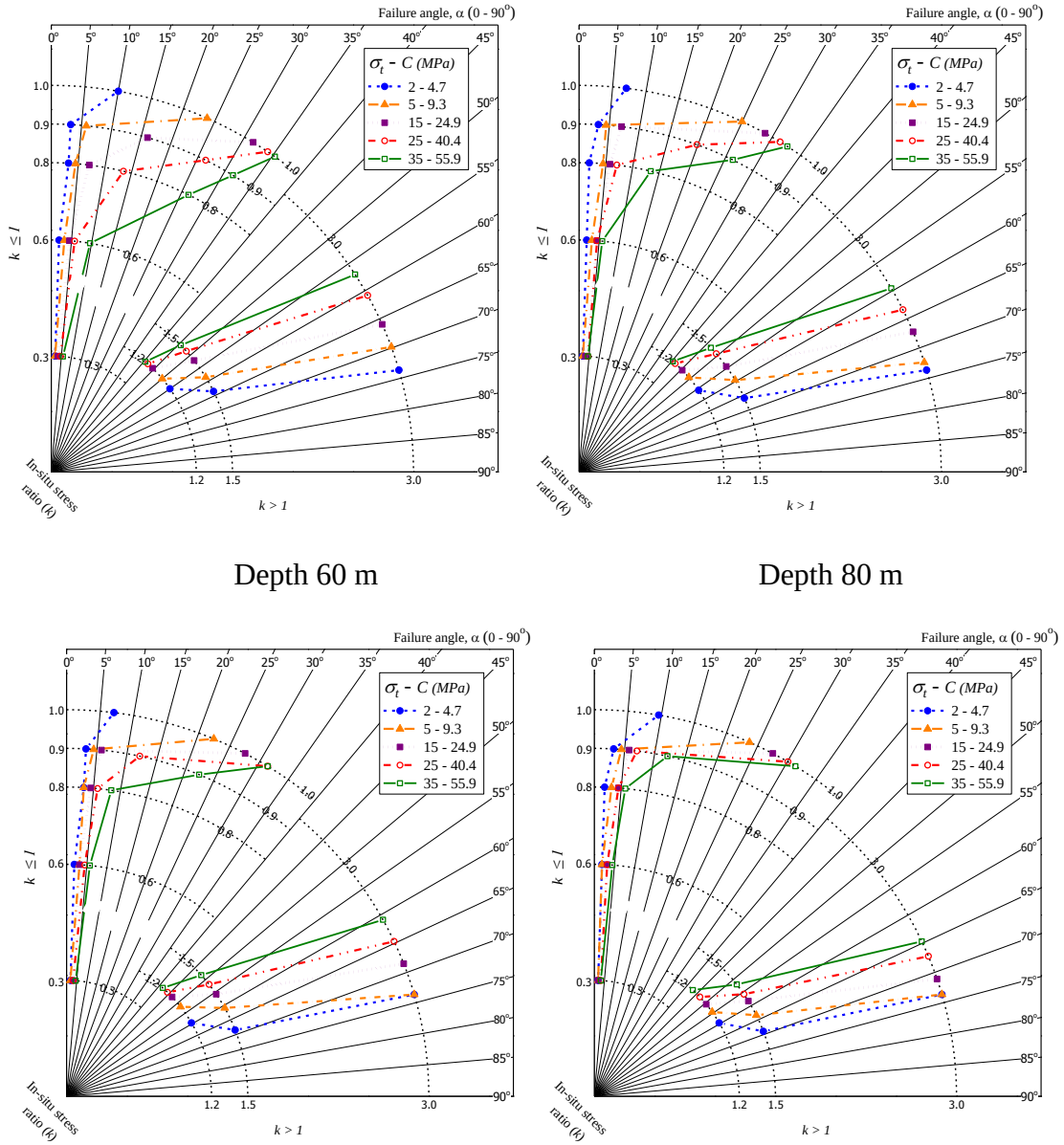

Figure 4.11 The transition of the crack initiation location against rock strength

4.3 Preliminary evaluation on failure patterns

The analysis results of evaluation of crack initiation in previous section indicates that, with various rock strength properties and diferent *k* values, the crack initiation point and corresponding failure mode can be varied. It is then of interest if the crack propagation will be also varied with various rock strength properties. In this section, the preliminary evaluation of failure path is carried out. Since it is impossible to analyse all cases considered for evaluation of crack initiation, therefore, careful consideration for selection of cases to be studied, is of importance.

The concept of case selection is to cover all possible behaviors that may occur. Therefore, the grouping concept is chosen here. The idea is to group the cases that have similar crack initiation points and similar initial crack modes and directions. The crack initiation points and modes have been already obtained from the previous section. The initial crack direction which still has no information, is then preliminary evaluated from the trajectories of principal stresses. By using these concepts, we plotted the crack initiation point together with corresponding trajectories of principal stresses in the near-field zone. In addition, the estimated possible failure paths are also included in the plot. The preliminary analyses showing the failure path patterns for both failure modes together with trajectories of principal stresses for cases with various *k* and rock strength values are illustrated in Figures 4.13-4.21. For Figures 4.13-4.18 (8 Figures for 8 different k), Figure a is for rock that provides the minimum value of rock strength. On the other hand, Figure b is for rock that provides the maximum value of rock strength. These minimum and maximum values refer to the possible values of natural rocks. The crack initiation points for both values are illustrated in Figure 4.12.

It is noted that this consideration is also related to the cavern pressure. For rock having minimum rock strength value, the cavern pressure to induce the initial crack would be less than that of rock having higher strength. The level of cavern pressure will result to changes in patterns of trajectories of principal stresses. Not only the different failure paths, but also the development of the trajectories of principal stresses (due to changes of level of cavern pressure) can be seen from the Figures. These can assist the grouping.

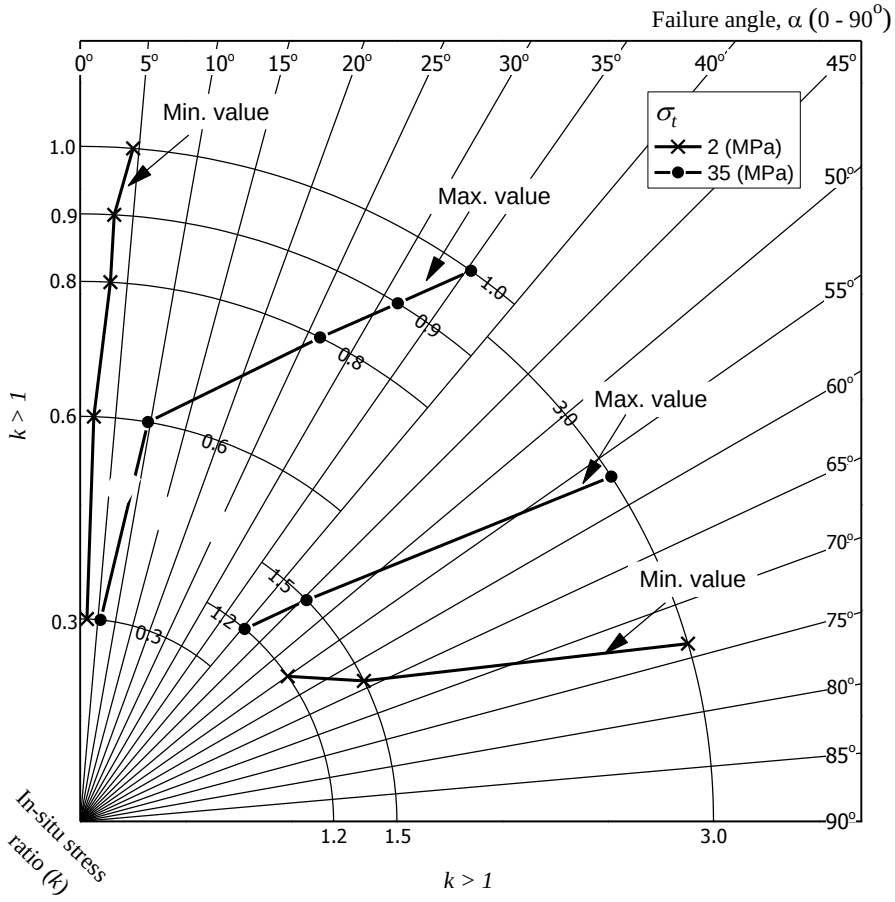

Figure 4.12 Initial crack point considered by minimum and maximum rock strength

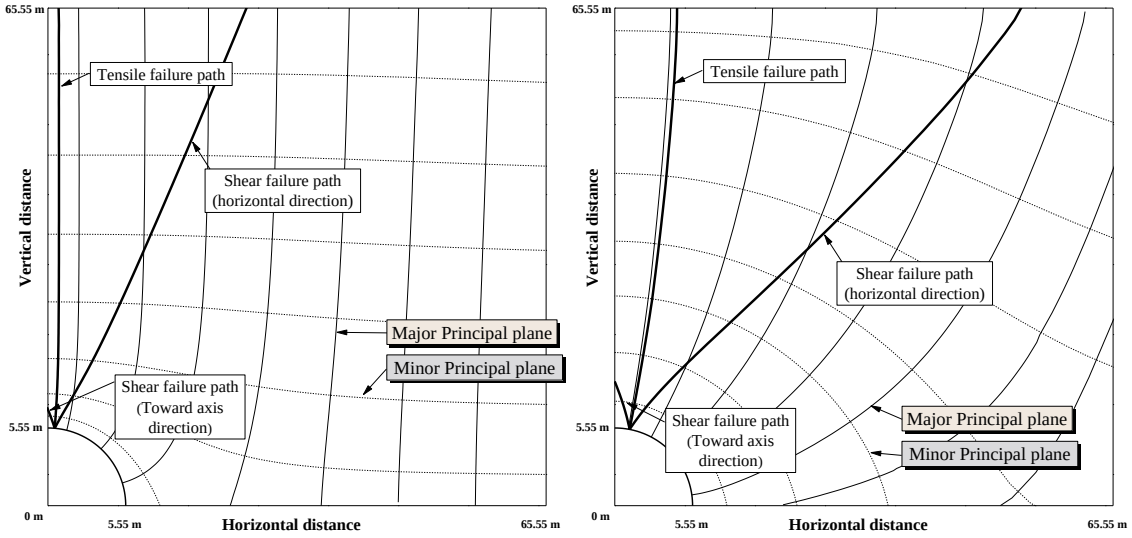

Figure 4.13 Estimated failure pahts pattern and Trajectories of principal stresses for *k* of 0.3 (scale x:y =1:1)

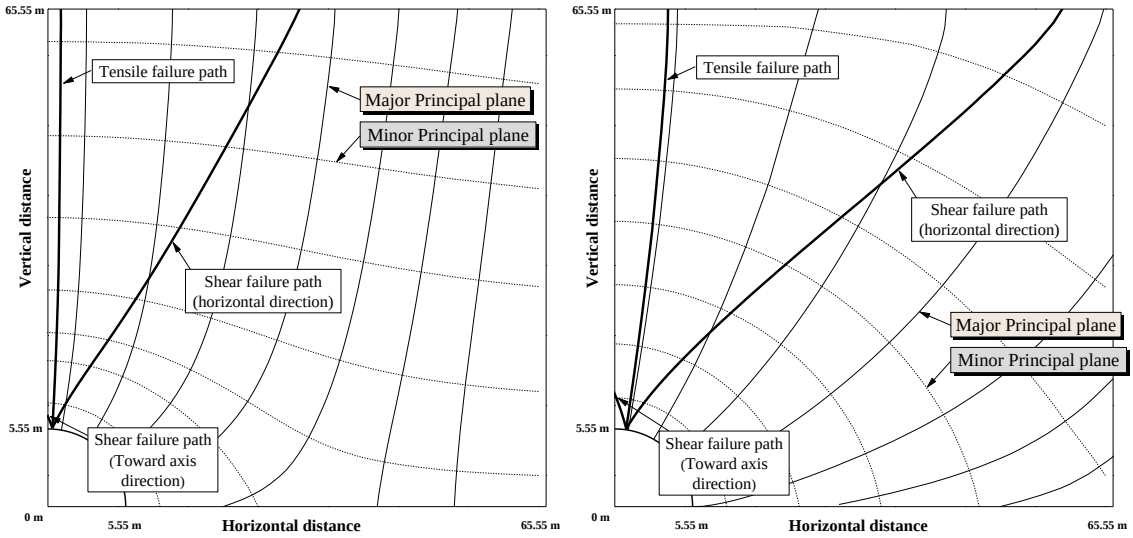

Figure 4.14 Estimated failure pahts pattern and Trajectories of principal stresses for *k* of 0.6 (scale x:y =1:1)

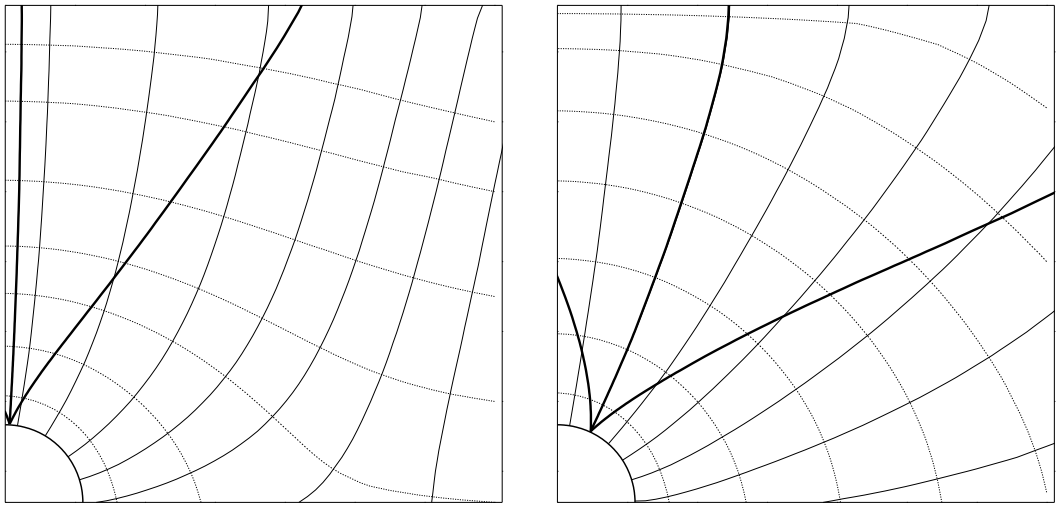

a) b)

Figure 4.15 Estimated failure pahts pattern and Trajectories of principal stresses for *k* of 0.8 (scale x:y =1:1)

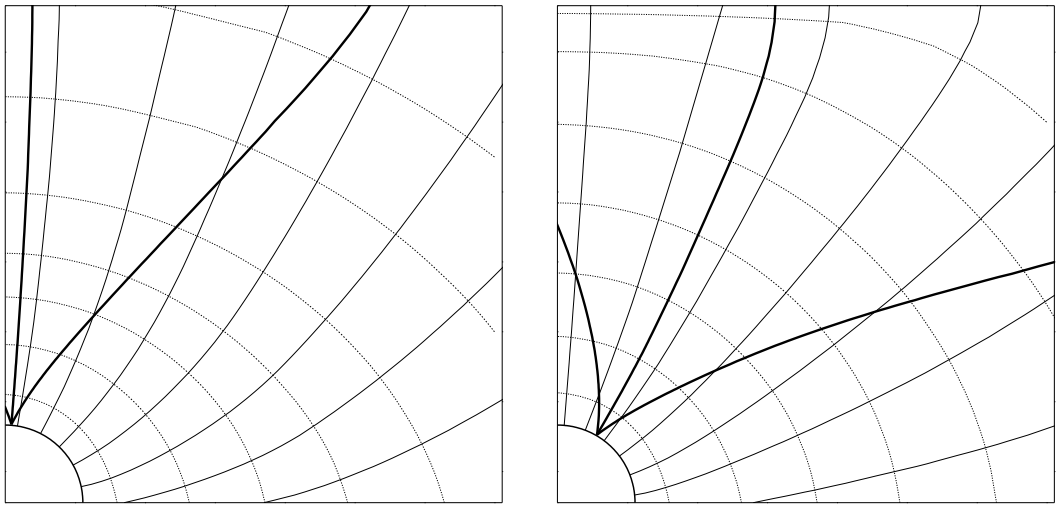

a) b)

Figure 4.16 Estimated failure pahts pattern and Trajectories of principal stresses for *k* of 0.9 (scale x:y =1:1)

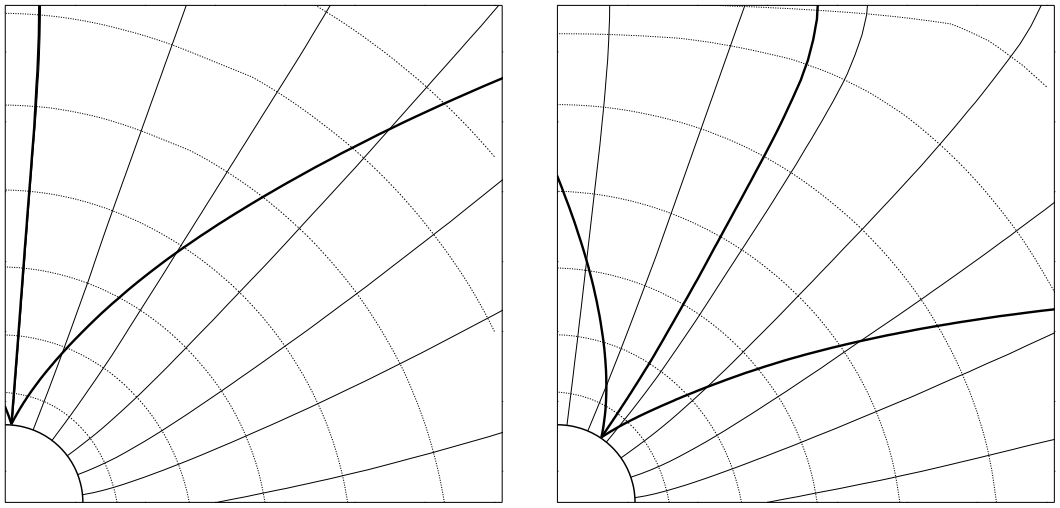

a) b)

Figure 4.17 Estimated failure pahts pattern and Trajectories of principal stresses for *k* of 1 (scale x:y =1:1)

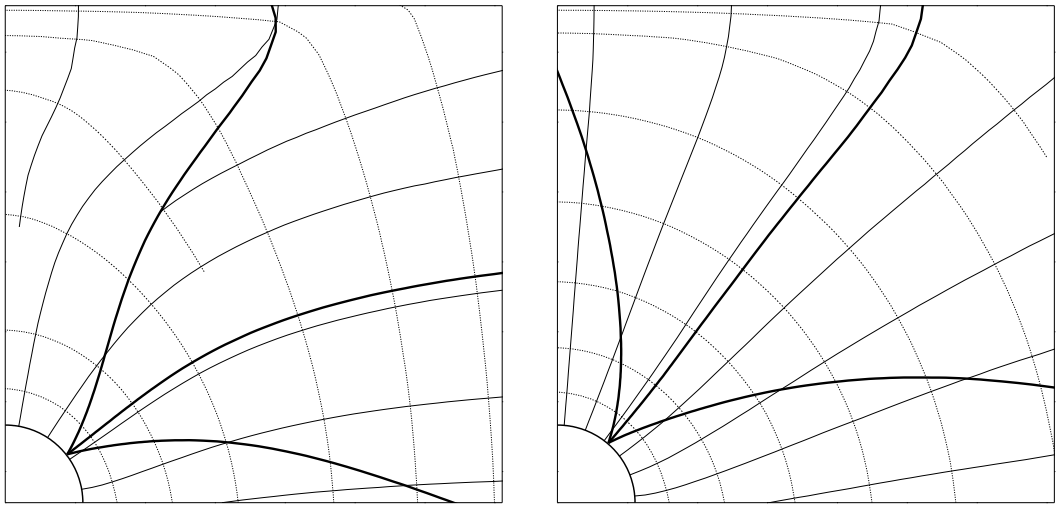

a) b)

Figure 4.18 Estimated failure pahts pattern and Trajectories of principal stresses for *k* of 1.2 (scale x:y =1:1)

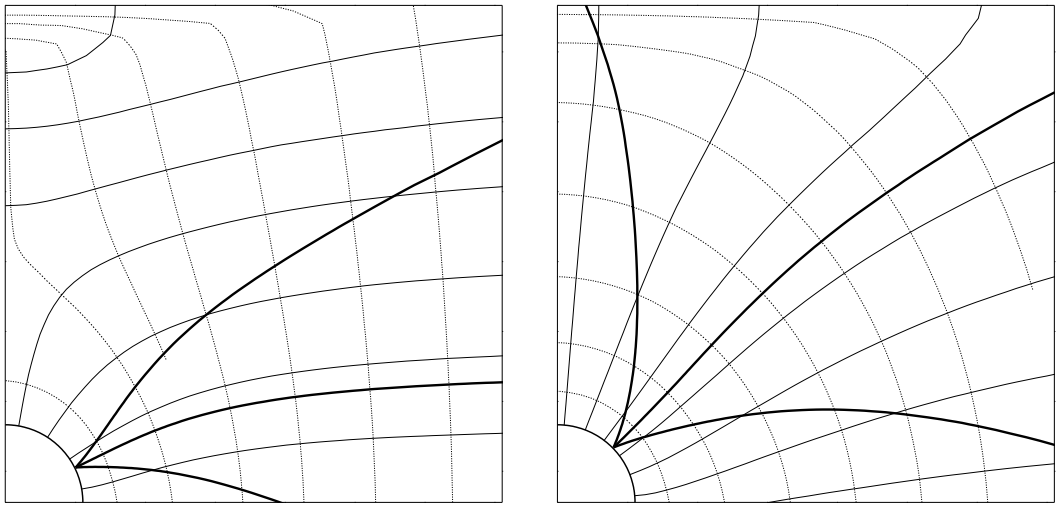

a) b)

Figure 4.19 Estimated failure pahts pattern and Trajectories of principal stresses for *k* of 1.5 (scale x:y =1:1)

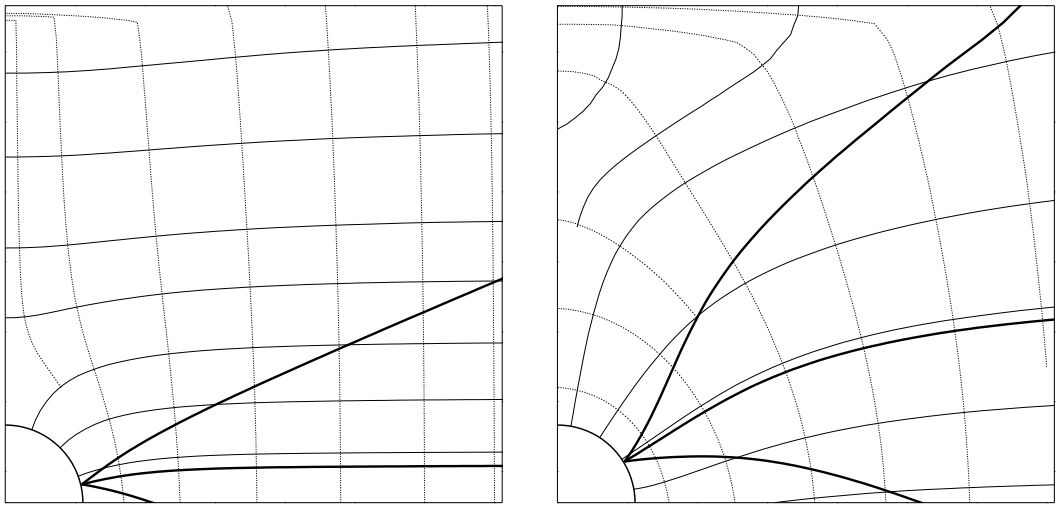

a) b)

Figure 4.20 Estimated failure pahts pattern and Trajectories of principal stresses for *k* of 3 (scale x:y =1:1)

From consideration of all Figures, it is found that;

1. The patterns of trajectories of principal stresses for cases with different *k* become different. These are due to different stress state or level of internal stress to induce crack initiation, which in turn, depend on the rock strength.

2. The patterns of trajectories of principal stresses for cases of $k \leq 1$ and $k > 1$ are clearly different for rock with low strength (having low cavern pressure to induce crack initiation). This becomes distinct when comparing the cases of $k = 0.3$ and 3. For case of

k = 0.3, the tensile plane aligns vertically. In contrast, the horizontal tensile plane is captured for case with *k* = 3.

3. For high strength rock which needs high cavern pressure to induce crack initiation, the patterns of trajectories of principal stresses for cases of *k* in the range of 0.8 -1.5 become similar to those of case with *k* =1.

With consideration in terms of crack initiation point and failure paths, the following are observed.

1) For low strength rock, the *k* has strong influence on failure path. For *k* equals or less than 1, the crack initiations are located at the cavern crown having the failure angle in the range of 2-10 °. The trajectories of the minor principal stress are directly upward to the ground surface, of which their trajectories near the tunnel zone are initially perpendicular to the cavern wall and then tend to upward to ground surface at far field. In contrast, for *k* larger than 1, the trajectories of the minor principal stress around the cavern are still initially perpendicular to the cavern surface but their trajectories are in the horizontal direction for far field. The range of failure angle in this situation is of 50-70 °.

2) For high strength rocks, the influence of *k* becomes smaller. Since, it requires a high level of internal pressure to induce the failure initiation. Therefore, the stresses in the near-field are governed by the internal pressure. The direction of major principal stress is then in radial direction (direction of cavern pressure) as seen in the Figures. Consequently, the possible tensile failure plane is thus in radial direction. With the crack initiation at around 40 ° from cavern crown, the possible tensile failure path in this case aligns as inclined line with 40 ° with horizontal plane. Therefore, the third group for case selection represents for high strength rocks having *k* in the range of 0.8-1.5.

Moreover, 3) for high strength rocks with *k* of 0.3 and 0.6, the influence of *k* on the trajectories and failure path can be still observed. The crack initiation point always occurs at the cavern crown. The patterns of trajectories of principal stresses are similar to those of low strength rock. Therefore, the high strength rock with low *k* is classified in the first group. While, the high strength rock with very high *k* (k= 3) is classified in the second group.

From the above-mentioned discussion, 3 groups which have different patterns of trajectories of principal stresses, crack initiation points and failure path characteristics, can be summarized as follows;

Group 1: Low strength rocks with *k* equals or less than 1 and high strength rocks with small *k* (k = 0.3-0.6)

Group 2: Low strength rocks with *k* larger than 1 and high strength rocks with very high *k* (k = 3)

Group 3: High strength rocks with *k* in the range of 0.8 - 1.5

For Groups 1 and 2, the *k* has strong influence on both crack initiation and failure path characteristics. For Group 3, the crack initiation point is around at 40 ° from cavern roof and the failure path aligns in radial direction. The behavior is governed from high cavern pressure, not the in-situ stress.

4.4 Failure mode of fracture propagation

In this section, the failure modes (tensile and shear) of fracture propagation in rock masses around pressurized gas storage cavern are of interest. It consists of three parts which are case selection, progressive failure analysis and verification case with previous study (Tunsakul et al., 2013).

After the evaluation of crack initiation was obtained in section 4.2, those results revealed that either shear and tensile would be occurred depending on the relationship between the σ_t and C. As described in section 4.2, when the relationship between σ_t and C locates above the line of D/R=1, the failure is initiated with tensile mode. Thus, the tensile fracture mode is expected. While a pair of C - σ_t situates under the line of D/R=1, shear fracture mode is expected. Therefore, the analysis in this section is to further investigate that, with tensile and shear crack initiation, the crack will propagate with tensile or shear modes by the simulation of contact-friction interface.

In the simulation with interface as mentioned in section 3.5, three pre-determined failure paths (two failure modes) are prepared in the FE mesh (first remeshing). The prepared failure paths are then to be investigated whether which path and failure mode the crack would propagate. By repeating these procedures, three pre-determined failure paths at a new crack tip are consequently calculated and prepared in the FE mesh (second remeshing). The change of failure mode can be then investigated again. In order to verify the concept in this study, the rock strength parameters herein are carefully selected with respect to the line of D/R=1 so as to investigate this issue. In addition, the changing orientation of failure path during crack propagation, is the well-recognized in fracture propagation problem. The investigation is also performed in this study.

Therefore, the investigation in this section starts with evaluation of initial failure path following with possibility on change of failure mode. Finally the change of crack propagation path is investigated.

4.4.1 Case selection

Figure 4.21 shows 6 analysis cases with careful selection on the chart of the line of D/R=1. This Figure is also used to explain how six analysis cases are to be selected.

First, it is necessary to select σ_t two values of 2 and 15 MPa in order to select the suitable analysis cases. After that the two values of C, 4.7 and 24.9 are obtained by D/R=1 equation (from section 4.2.1). The relationships of two points in σ_t – C space are shown at point (a) and (b). Based on the concept of the D/R=1, both situations at point (a) and (b) are lined on the line of D/R=1, it means that during the increasing of cavern pressure, the stresses state at initial crack of both situation are about to reach both tensile and shear failure criteria at the same time.

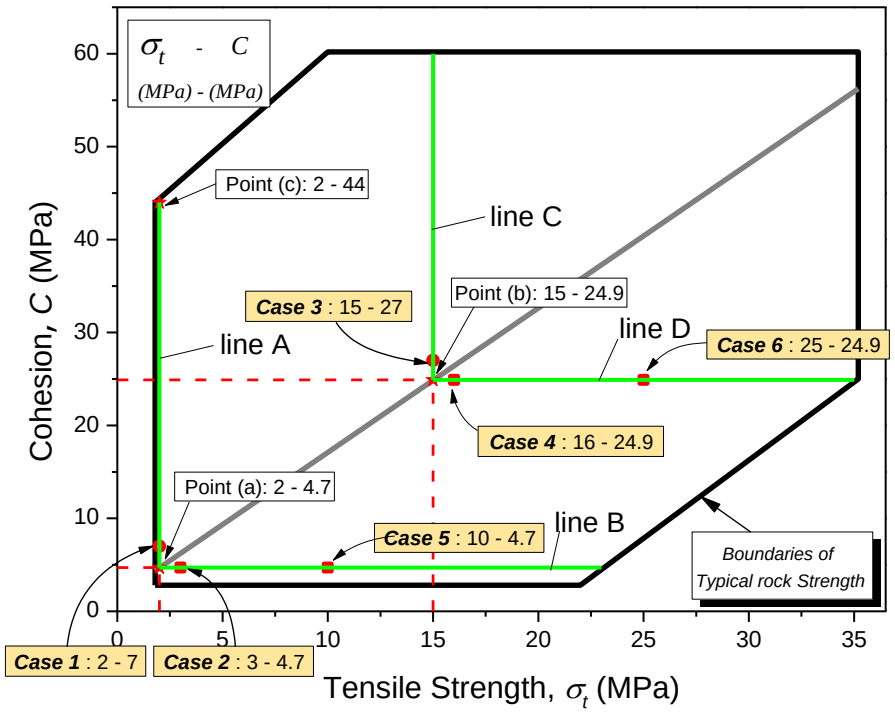

Figure 4.21 Six analysis cases in the $\sigma_t - C$ space with the concept of D/R=1

Figure 4.22 shows the situations of the stress state reaching both tensile and shear criteria for the rock strength at point (a) and (b) that presented by the contour of σ_1 and contour of D/R.

For point (a), it is found that at the level of cavern pressure of 9 MPa induced the maximum σ_1 of 2.46 MPa and minimum D/R of 0.99. The failure angle of 10° is indicated for initial crack position. The maximum σ_1 of 15.32 MPa, minimum of D/R of 1.00 and failure angle at 33 ° are observed by cavern pressure of 30 MPa for point (b).

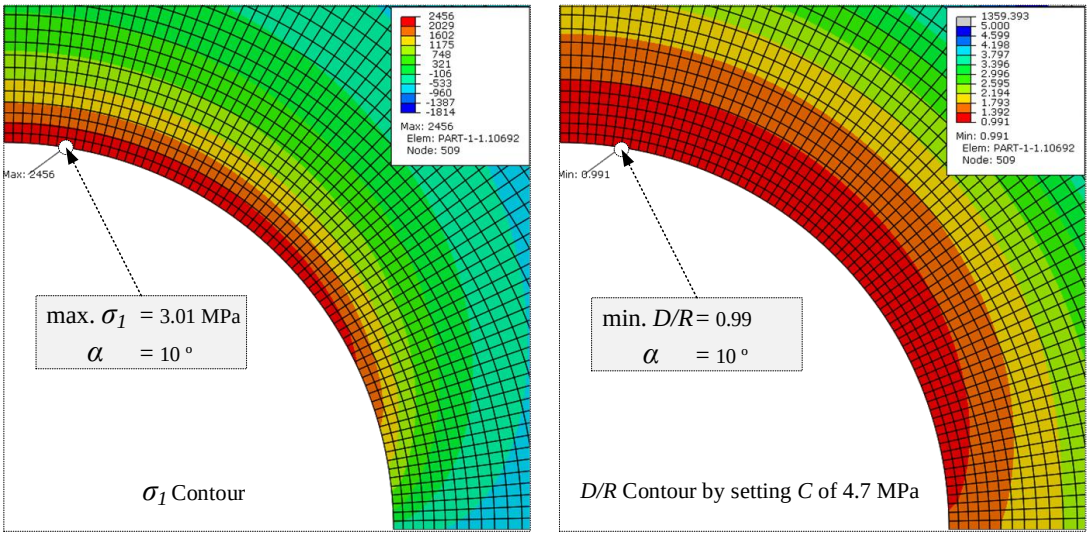

(a) At cavern pressure of 9 MPa

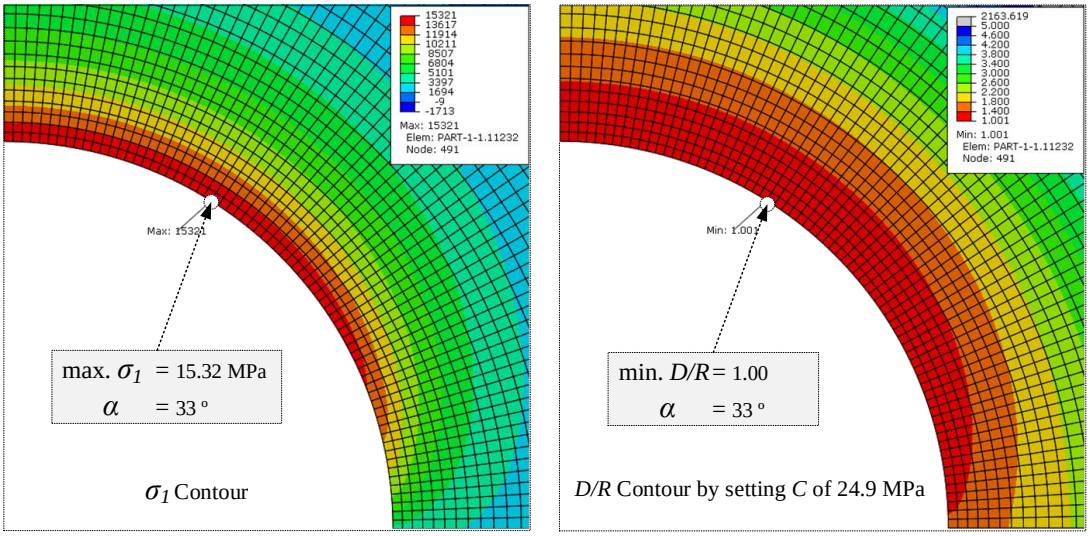

(b) At cavern pressure of 30 MPa

Figure 4.22 Contours of major principal stress and D/R at different cavern pressures

Then, the procedure for prediction of three failure paths are to be performed (section 3.3) by calculation which using the stress state at initial crack for points (a) and (b) (at level of cavern pressure of 9 and 3 MPa, respectively). Two patterns of possible failure paths are obtained for points (a) and (b) as shown in Figure 4.23 (a) and (b).

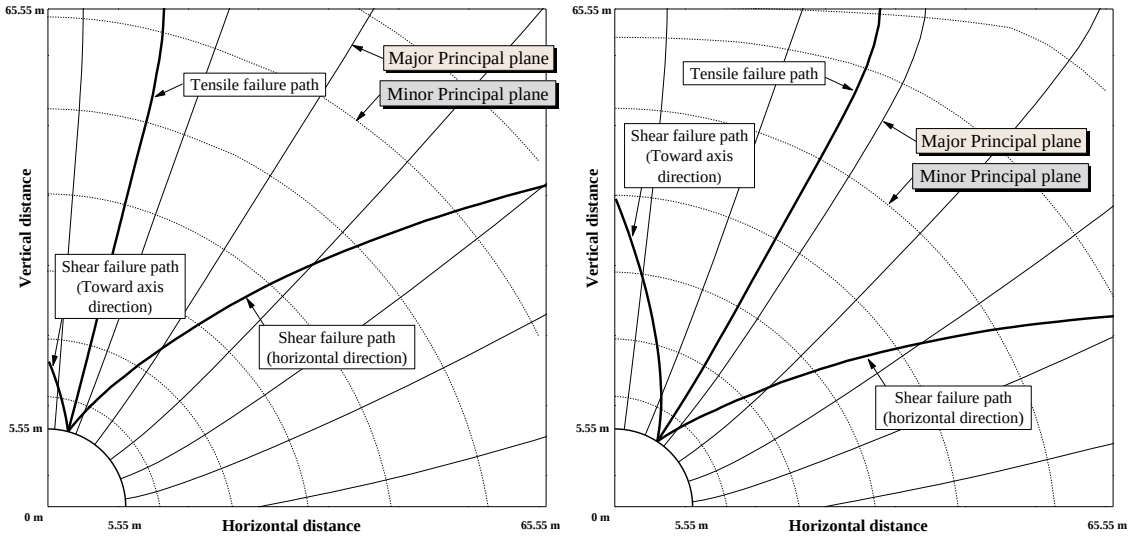

(a)
10 ° (σ_t =2, C = 4.7)
(Predicted by Cavern pressure of 9 MPa)

(b)
33 ° (σ_t =10, C = 24.9)
(Predicted by Cavern pressure of 30 MPa)

Figure 4.23 Prediction of possible failure paths (scale x:y =1:1)

The parameters (relationship of σ_t and C) that can be applicable for both predicted patterns of failure paths (Figure 4.23 a) and b)), are discussed by the concept of the line of D/R=1 in the Figure 4.21.

By observation in Figure 4.21, the values of σ_t and C on lines A, B, C and D can be identified as follows,

A, σ_t = 2 and C > 4.7– 44 (constant σ_t at 2)
B, σ_t > 2 – 23 and C= 4.7 (constant C at 4.7)
C, σ_t = 15 and C > 24.9 – 60 (constant σ_t at 15)
D, σ_t > 15 – 35 and C= 24.9 (constant C at 24.9)

Considering the concept of the line D/R=1, the relationship between σ_t and C lined on the straight line, along A and B can be only used as input parameters in the failure pattern at 10 ° for initial crack point (Figure 4.23 (a)). It is due to that only tensile failure criterion shall be satisfied along the line A by the level of cavern pressure of 9 MPa (selected σ_t of 2 compares with occurring for σ_1 of 2.3 MPa, thus, only tensile mode is satisfied because of value of C on A line > 4.7– 44). In contrast, along the line B, the stress state induced by cavern pressure of 9 MPa reach only shear failure criterion (D/R=1 at C= 4.7 MPa, thus, only shear mode is satisfied, because of σ_t on B line > 2 – 23). As the same reason, the relationship of σ_t and C located on the lines C and D are able to use as the input parameters for this failure path (initial crack at 33°) in the Figure 4.23 (b).

It is noted that the relationship of σ_t and C located on *the dash* line in Figure 4.21 is not applicable for those two failure paths (initial crack point at 10 and 33°). For example, point (c) (σ_t = 5 and C = 24.9) on read dash line in Figure 4.21), will reach the tensile failure (σ_t of 5 MPa) at different internal pressure and the failure angle will be not at 10 and 33°.

In fact the Chart D/R=1 is originally developed to distinguish the failure initiation mode. For evaluation of failure propagation mode, it is then doubted that this concept is still applicable or not. Therefore, further study is carried out. The relationship between σ_t and C for this purpose is therefore carefully selected. Pairs of σ_t-C which are both close and far from line of D/R=1 should be considered. It is assumed that the failure propagation mode will be compatible with failure initiation mode if a pair of σ_t-C is far from the line. While the failure propagation mode can be different from that of initiation for cases with pair of σ_t-C is close to the line. Cases in this study will cover for both considerations.

To fulfill that, pairs of σ_t-C which are both close and far from the line are selected. Cases 1-4 are represented for pairs of σ_t-C which are close from the line. Whereas, cases 5 and 6 are for pairs of σ_t-C which are far from the line. It is noted that both cases 5 and 6 represent for shear failure initiation. The analysis results for cases 1-4 reveal that the fracture initiates with tensile mode will prolong propagating with tensile fracture. While the fracture which is initiated by shear failure, can propagate under either shear or tensile mode (see in next part). All analysis cases are tabulated in Table 4.2 with necessary information including initial crack point, σ_t, C, k and expected fracture mode for each case.

Table 4.2 All selected analysis cases

Case	Location approx. (°)	Rock Properties			Failure mode (expected)
		Tensile Strength (MPa)	Cohesion (MPa)	*k*	
1	10	2	7	1	Tension
2		3	4.5	1	Shear
3	33	15	27	1	Tension
4		15	24.9	1	Shear
5	10	10	4.5	1	Shear
6	33	25	24.9	1	Shear

4.4.2 Progressive failure analysis for the initial crack propagation

The objective of this section is to investigate the failure propagation by performing progressive failure analysis with remeshing technique. By this method, pre-determined possible failure paths (both failure modes) are prepared in advance by embedding the interface-contact interaction with rock strength parameters along those paths. The analysis is then re-performed with this new FE mesh. It can then be observed whether which failure path propagates.

Figure 4.24 shows the FE mesh modeling (first remeshing) of the possible failure paths which are obtained from stress state at crack initiation stress state (applied cavern pressure at 9 MPa) for the initial crack at failure angle of 10 ° (case 1, 2 and 5). For the initial crack at failure angle of 33 ° (case 3, 4 and 6), the FE mesh modeling is shown in Figure 4.25.

Three pre-determined failure paths are then prepared in the new FE mesh as shown in both figures. Along the prepared possible failure paths, two opposite sides of the region (which are divided by the failure paths) are connected with the contact-interface interaction with the behaviors specified in section 3.6. Those models are used to investigate whether which path the crack would propagate by embedding theirs rock strength properties for each case (1-6) along three pre-determined possible failure surfaces. The rock strength properties in case of 1, 2 and 5 are applied in the modeling in Figure 4.24, while case of 3, 4 and 6 are used in the modeling in Figure 4.25. By reanalysis with increasing of cavern pressure, crack propagation along one of the prepared failure path can be seen.

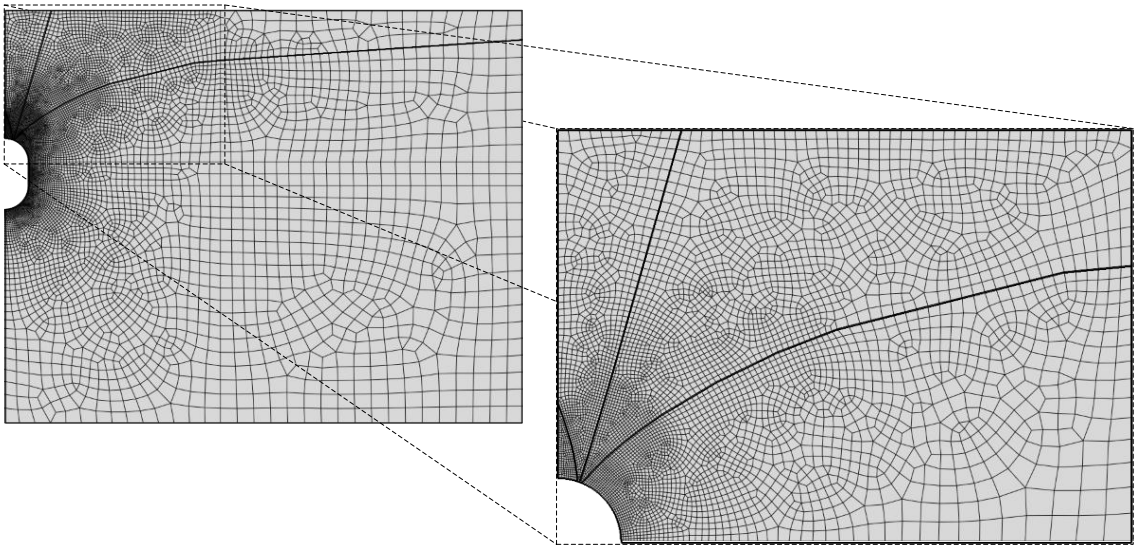

Figure 4.24 Model simulations with interface interaction for analyzing cases 1, 2 and 5 with initial crack at 10 ° (scale x:y =1:1)

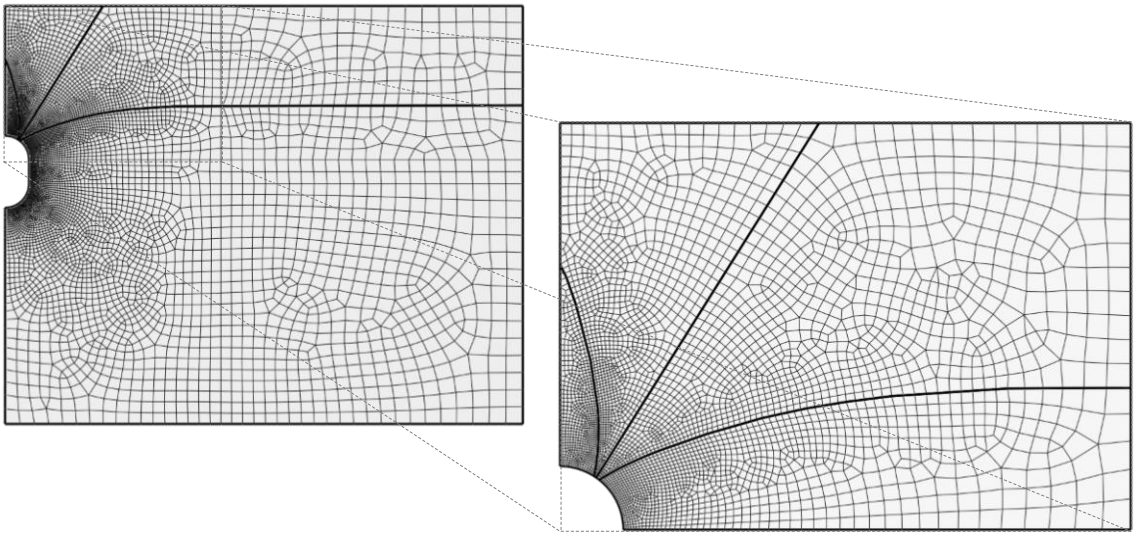

Figure 4.25 Model simulations with interface interaction for analyzing cases 3, 4 and 6 with initial crack at 33 ° (scale x:y =1:1)

The results of the analyses for each case in this section are illustrated as mesh deformation with σ_1 contour in the left side and D/R contours in the right side. The evolution of both contours is shown, which results from gradually increasing the cavern pressure with step by step for each selected cases. This increasing is also related to the induced of cavern pressure at initial crack for each cases.

Therefore, for cases 1, 2 and 5, the gradually increased of cavern pressure is carried on by increasing the cavern pressure of 9.0, 9.5, 10.0 and 10.5 MPa, respectively. While the applying of cavern pressure by 33, 34, 35 and 36 is for the analysis cases of 3, 4 and 6. In addition, it is essential to set the range of σ_1 and D/R contours with having correlation of their rock strengths (σ_t and C), in order to observe the stress redistribution for each cases.

1. Expected tensile fracture case

As mentioned in the previous section, cases 1 and 3 are expected for tensile fracture that since the relationship of σ_t –C is located above the line of D/R=1. The analysis is performed by with different the model simulations in Figures 4.25 (failure angle at 10 °) and 4.26 (failure angle at 33 °) for cases 1 and 3, respectively. The results of cases 1 and 3 are shown in Figures 4.28 and 4.29.

Figures 4.28 and 4.29, with gradually increasing the cavern pressure, it was clearly seen that crack propagation along tensile failure path was observed. In addition, by observation of σ_1 contours, on the left side of both figures, the redistribution of σ_1 could be noticed. At certain levels of cavern pressure, the evolution of σ_1 around a crack tip along the tensile failure path almost reaches the σ_t (black). It means that the tensile fracture is ready to prolong propagating if the cavern pressure increases. In contrast, the D/R contours for both cases (on the right side) reveals that it still remains with values larger than 1.).

Besides, during increasing cavern pressure, the contour of σ_1 indicates that the values at some positions (α of 50° for case 1 and 70° for case 3) along cavern surface exceed σ_t. This implies that the new crack may generate. On contrary, the D/R contour along cavern surface indicates no new crack occurrence.

It is noted that the intensity of σ_1 contours are illustrated by considering the relationship between σ_t and C. For example, for case 1, σ_t and C of 2 and 7 MPa, the range of σ_1 contours are set to illustrate by 0 (white) – 2 (black) MPa. For D/R contours are always by 1 (black) – 1.5 (white) with its calculation with its C value. The black color for both contours refer to reaching the tensile and shear criteria.

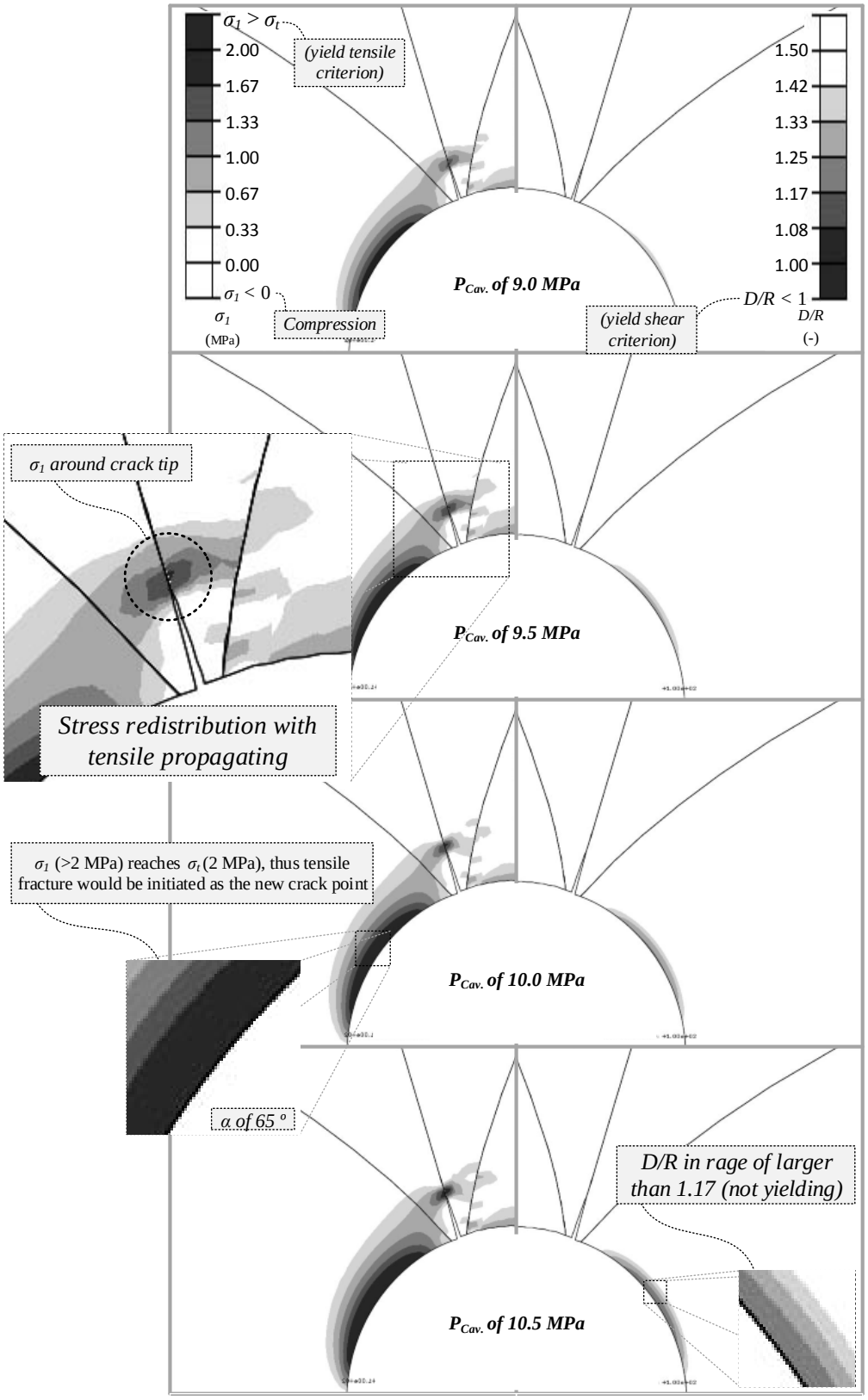

a)
σ_1 Contour
(Emphasis on Max. Scale of 2 MPa)

b)
D/R Contour by setting C of 7.0 Mpa
(Emphasis on Min. Scale of 1)

Figure 4.26 Analysis results for case 1: σ_t = 2 MPa, and C = 7 MPa (Tensile fracture is expected)

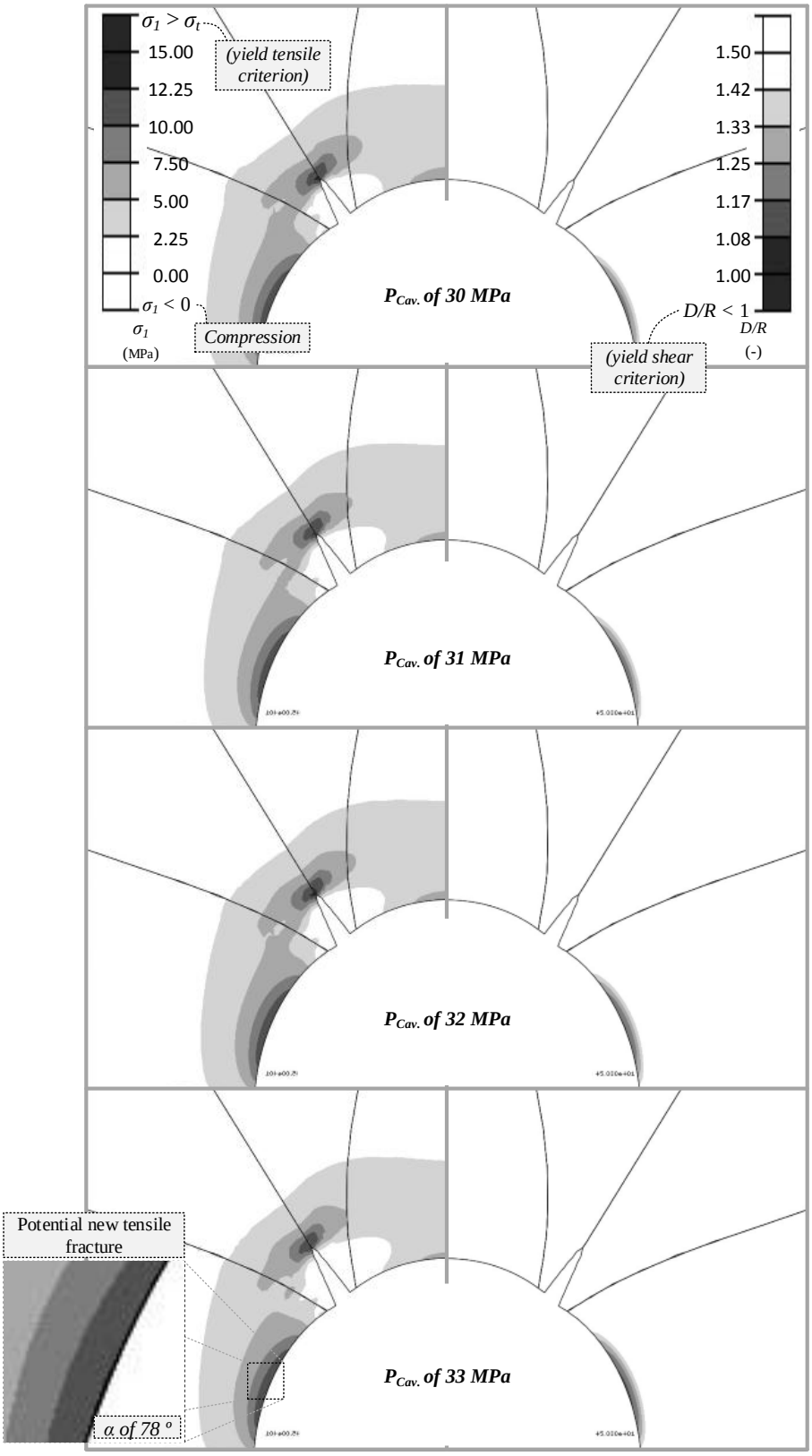

a)
σ_1 Contour
(Emphasis on Max. Scale of 15 MPa)

b)
D/R Contour by setting *C* of 27 MPa
(Emphasis on Min. Scale of 1)

Figure 4.27 Analysis results for case 3: σ_t = 15 MPa, and C = 27 MPa (Tensile fracture is expected)

2. Expected shear fracture case

The results in this section, shear fracture is expected to be observed. Cases 2 and 4 are performed in progressive failure analysis. The rock strength properties of each case are applied in the model simulation in Figures 4.24 and 4.25, respectively.

The results of cases 2 and 4 which the shear fracture is expected, were found that three potential failure paths are propagated concurrently as shown in Figures 4.28 and 4.29. By observing the contours of σ_1 and D/R correlating of their rock strengths (σ_t and C), the black color is occurred in both contours and getting more in black color during the gradual increase of cavern pressure. With the complicate results obtained, it is difficult to conclude, however, it may be interpreted that the fracture has initiated with shear and then it can propagate under either shear or tensile mode. However, since the pair of (σ_t , C) is close to the line D/R=1 even though it is located in shear failure initiation zone, the incremental stresses to induce each failure criteria are nearly the same. Moreover, there may be the effect of stress redistribution, particularly for shear failure. With the limitation of FEM used, details of fracture propagation in small increment cannot be captured. More advanced analysis method is necessary.

In addition, by considering the line of D/R=1 concept, cases 2 and 4 initiates with shear mode of which the pairs of C and σ_t are close to the line of D/R=1. As a results, it is probably because the rock has not high σ_t enough for suppression the tensile fracture. Therefore, a pair of C and σ_t that is far from the line of D/R=1 is further taken into consideration. The analysis cases 5 and 6 are extended to be selected so as to investigate only shear fracture with selecting σ_t far from the line. Case 5 is for σ_t and C of 10 and 4.7 MPa (see in Figure 4.21). It is initiated with shear failure mode at 10 ° of failure angle. Thus, this relationship is applicable for the model simulation in Figure 4.24. In the analysis case 6 with C of 24 and σ_t of 25 MPa, only shear mode is reached its criterion at the failure angle of 33°. Therefore, the model simulation in Figure 4.25 is used for the pair of C and σ_t in case 6 in order to observe the behaviors.

The results of cases 5 and 6 are shown in Figures 4.30 and 4.31. It was revealed that only shear fracture was propagated. Only the propagation of the shear failure plane that is close to the axis direction is noticed (which is not the shear plane in the horizontal direction). By considering σ_1 and D/R contours for tensile and shear mode, during the analysis, the D/R contours were illustrated in more black color, while the contours of σ_1 appears in grey color. It implies and confirms that the fracture was not propagated with tensile mode.

However, the results in term of deformed mesh of these cases are not distinguished to see the shear propagation with gradual increase of the cavern pressure. Because of the fact that shear behavior acts as a small sliding along the shear plane so that it is not clearly to be seen with shear propagation with a sliding behavior.

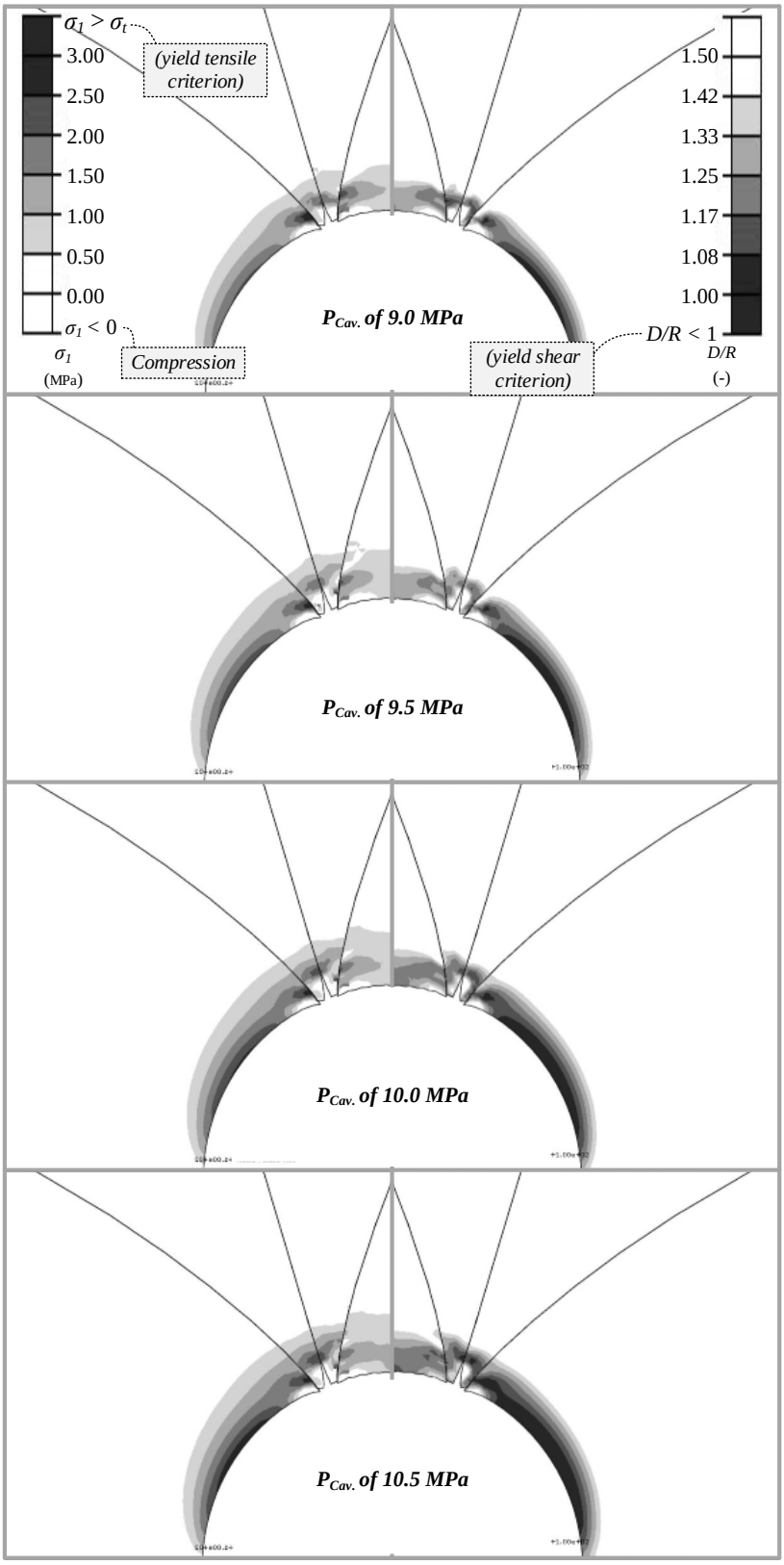

a)

σ_1 Contour
(Emphasis on Max. Scale of 3 MPa)

b)

D/R Contour by setting *C* of 4.7 Mpa
(Emphasis on Min. Scale of 1)

Figure 4.28 Analysis results for case 2 : σ_t = 3 MPa, and *C* = 4.5 MPa (Shear fracture is expected)

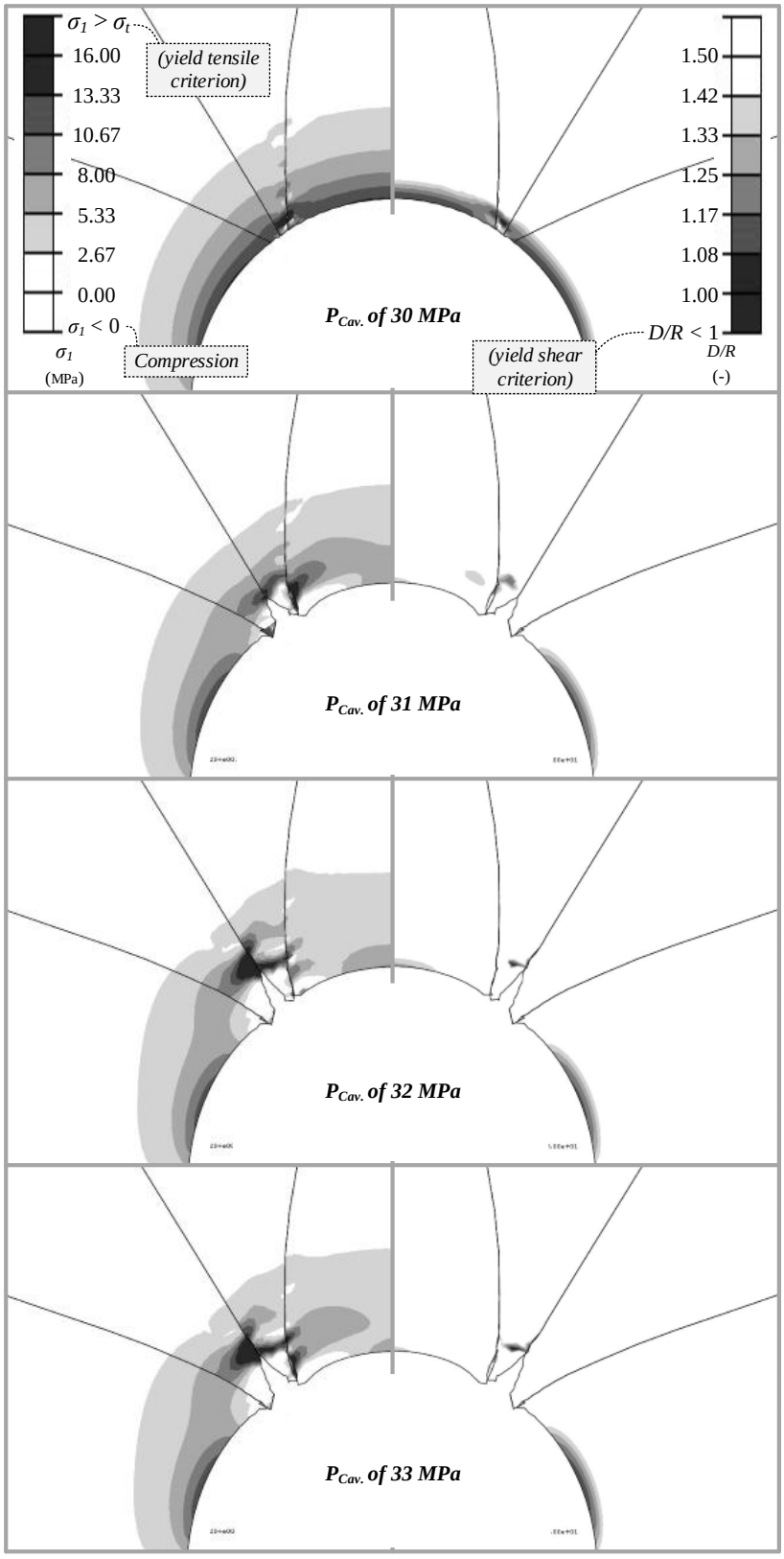

a)
σ_1 Contour
(Emphasis on Max. Scale of 16 MPa)

b)
D/R Contour by setting C of 24.9 Mpa
(Emphasis on Min. Scale of 1)

Figure 4.29 Analysis results for case 4: σ_t = 16 MPa, and C = 24.9 MPa (Shear fracture is expected)

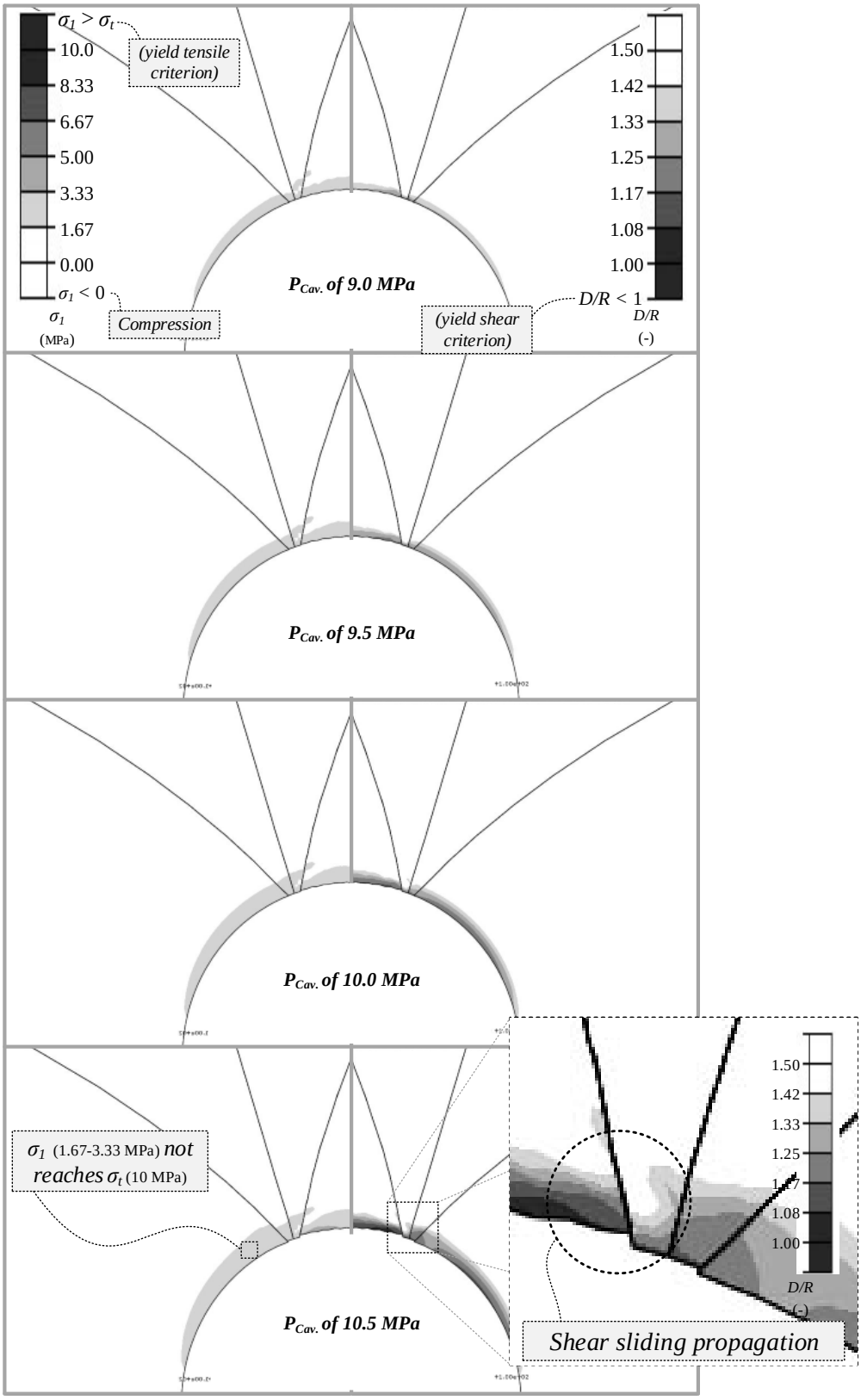

a)
σ_1 Contour
(Emphasis on Max. Scale of 10 MPa)

b)
D/R Contour by setting *C* of 4.7 Mpa
(Emphasis on Min. Scale of 1)

Figure 4.30 Analysis results for case 5: σ_t = 10 MPa, and C = 4.5 MPa (Shear fracture is expected)

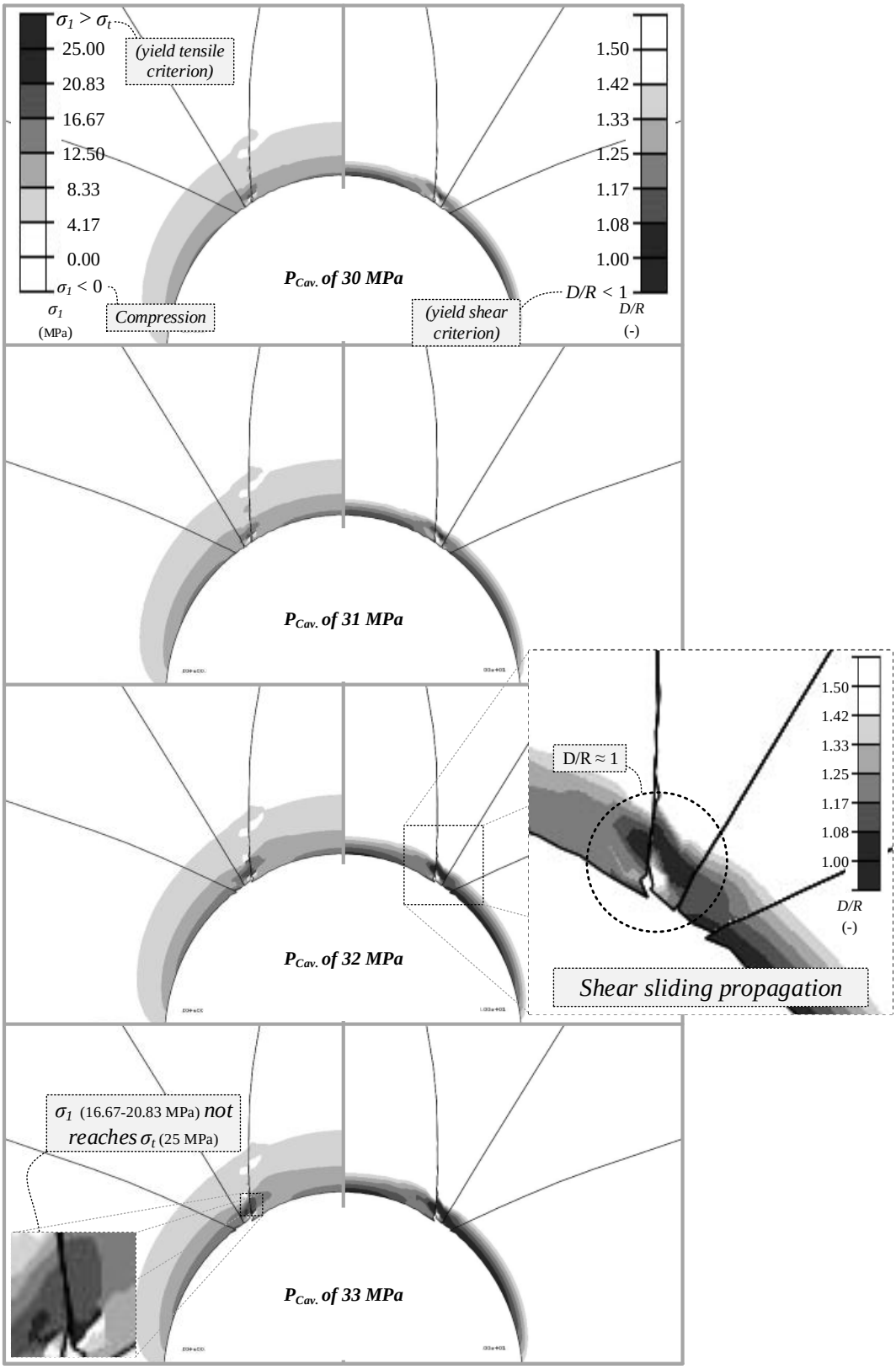

a)

σ_1 Contour
(Emphasis on Max. Scale of 25 MPa)

b)

D/R Contour by setting C of 24.9 Mpa
(Emphasis on Min. Scale of 1)

Figure 4.31 Analysis results for case 6: σ_t = 25 MPa, and C = 24.9 MPa (Shear fracture is expected)

4.4.3 Progressive failure analysis with considering the effect of stress redistribution

In the analyses in section 4.4.2, three pre-determined failure paths (two failure modes) were prepared in the FE mesh (first remeshing). The prepared failure paths were investigated whether which path and failure mode the crack would propagate. Those results are just only the initial propagation behaviors that are not considered the effect of stress redistribution. Commonly, during crack growing behaviors, the effect of stress redistribution is well-recognized in fracture propagation problem. In many researches (Tunsakul et al., 2013; Adachi, 1985, etc.) were found that the effect of stress redistribution has an impact on failure path propagation directions.

In addition, this study considers two failure modes (tension and shear) with three possible failure planes. Thus, it is due to the effect of stress redistribution, an assumption of interchanging between two failure modes is interesting for consideration. The interchange of failure modes here might change from tensile to shear or from shear to tensile.

Thus, the analyses in this section are to investigate the effect of the stress redistribution while the crack is growing on the interchanging failure modes and change of failure path orientation behaviors.

1. The interchanging of failure modes

In order to investigate the switching of failure modes, two cases with different initial failure modes (shear and tensile) are considered. Case 1 is selected as the representative of initial tensile fracture, whereas, the initial shear failure is represented by case 5. It is noted that the initial crack for both cases (1 and 5) are started at 10 degrees of failure angle and the model simulations in Figures 4.33 and 4.34 are reconsidered for this analysis.

By performing progressive failure analysis with remeshing technique, three failure planes for tensile and shear failure modes are still considered for these analyses. Thus, there are three possible failure paths which are calculated at any crack tip and then they are prepared in the FE mesh (second remeshing) for each cases. Figure 4.32 shows the new calculated of three failure paths. For analysis case 1 with initial crack propagation with tensile mode, the crack tip at the level of cavern pressure of 10 MPa is selected to calculate three possible failure paths. The patterns are used to simulate in the subsequent progressive analysis and its FE mesh for this case is shown in Figure 4.33. For initial crack propagation with shear mode of case 5, the crack tip at cavern pressure 10 MPa is selected to calculate the possible failure paths of which the patterns are used to generate the FE mesh. Figure 4.34 shows FE mesh model used for shear fracture in the reanalysis.

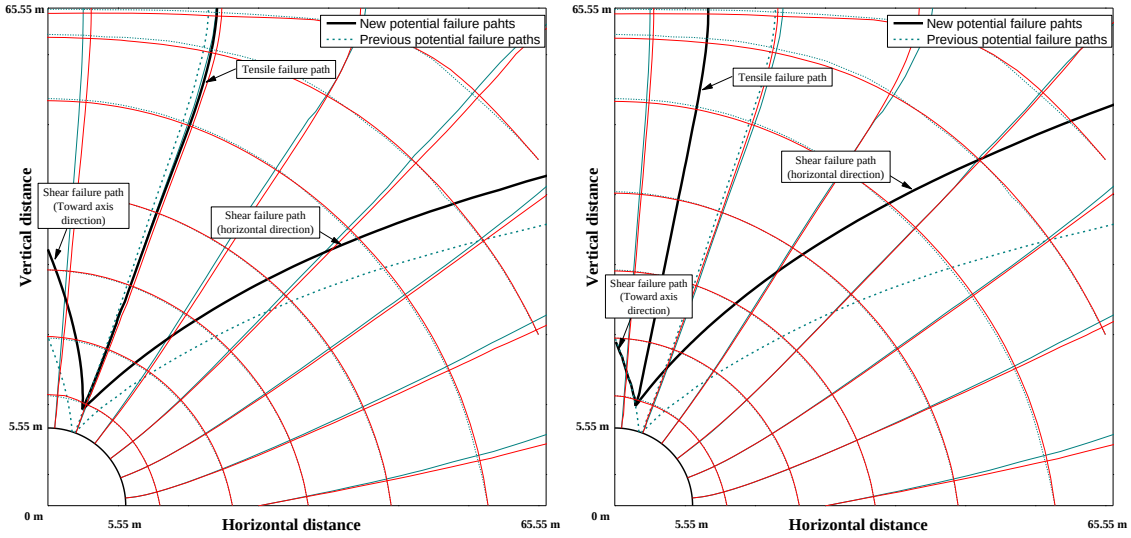

Figure 4.32 Selected possible failure paths after partial fracture propagation a) initial tensile failure b) initial shear failure (scale x:y =1:1)

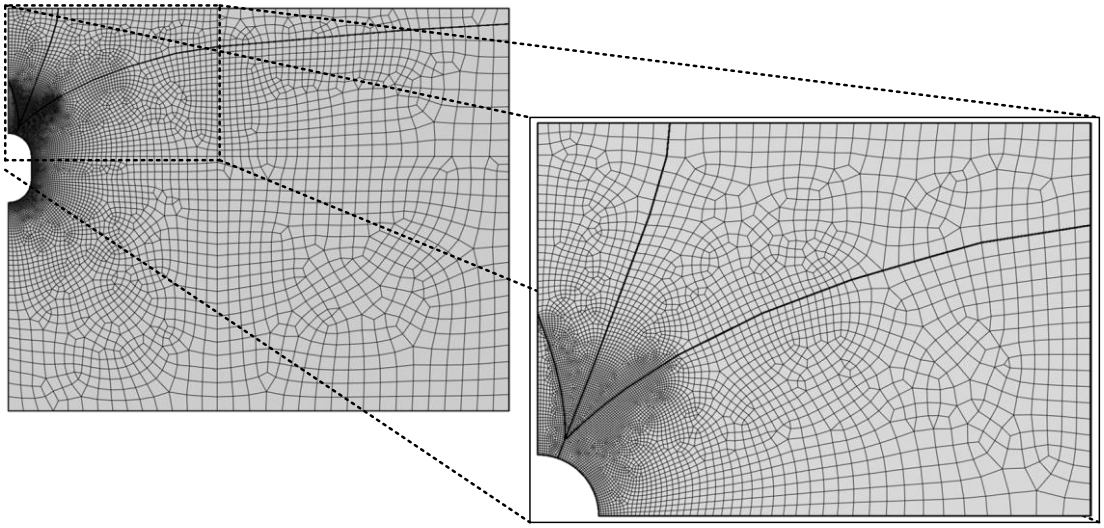

Figure 4.33 Model simulations with interface element after fracture propagation for tensile fracture case 1 (scale x:y =1:1)

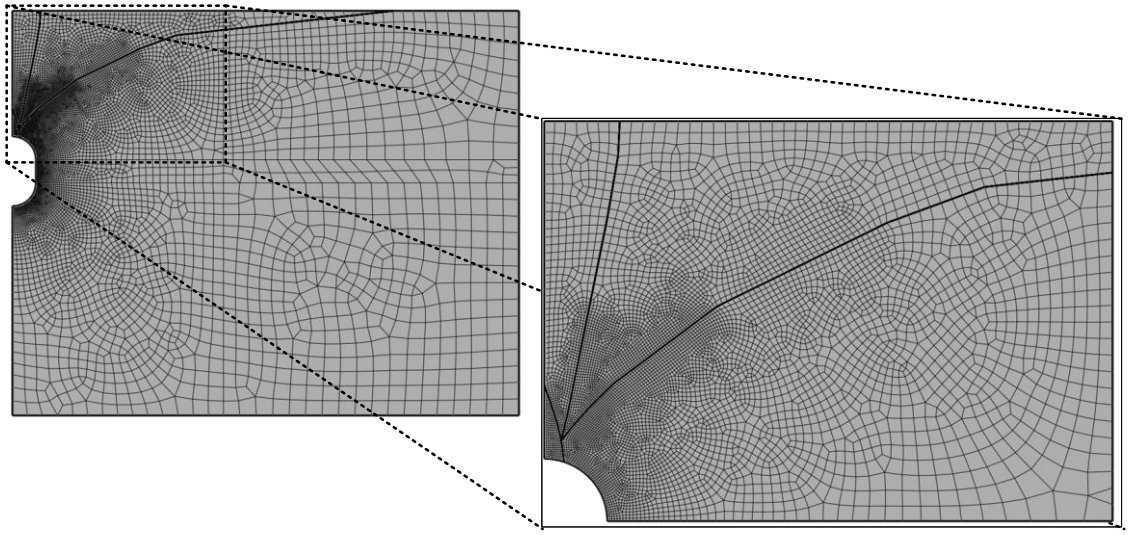

Figure 4.34 Model simulations with interface element after fracture propagation for tensile fracture case 1 (scale x:y =1:1)

Figure 4.35 shows the results of reanalysis with interface contact interaction with increasing of the cavern pressure for observing the change of failure mode. For initial tensile fracture case, it is seen that tensile failure path is continually prolonged and propagated along the prepared tensile failure path. Thus, the transition of failure mode from which the fracture starting with tensile failure changing to shear fracture is not happened.

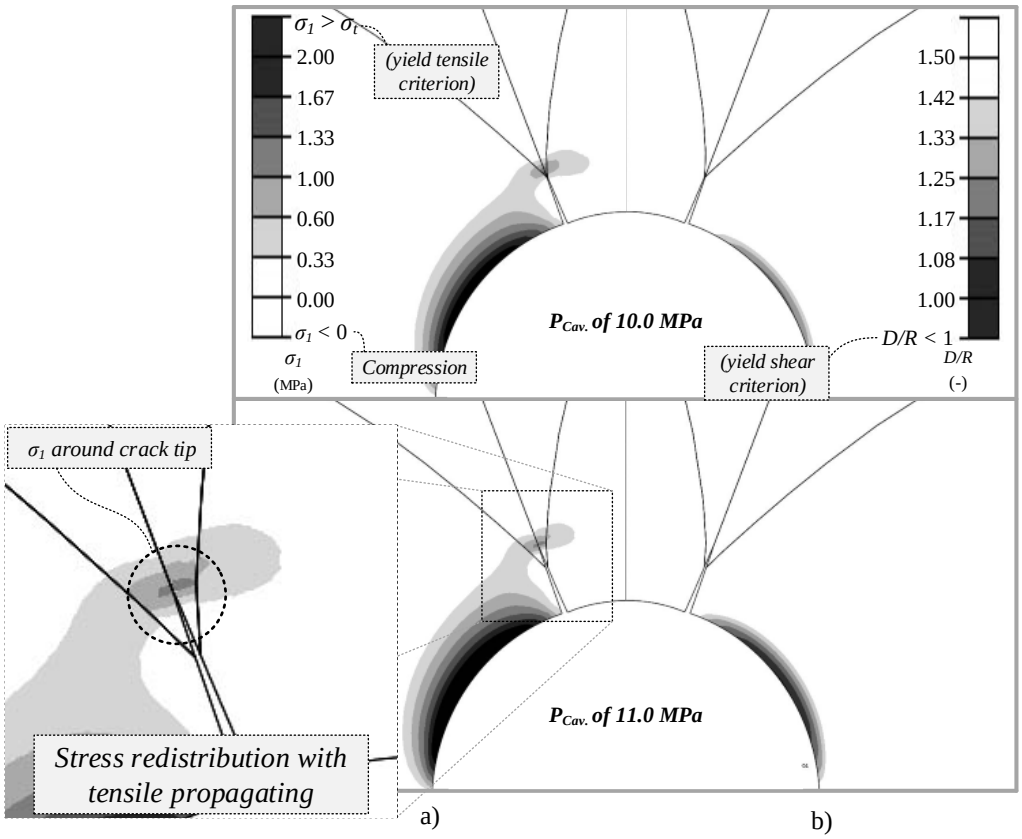

a) σ_1 Contour (Emphasis on Max. Scale of 2 MPa)

b) D/R Contour by setting *C* of 4.7 Mpa (Emphasis on Min. Scale of 1)

Figure 4. 35 Tensile fracture propagation

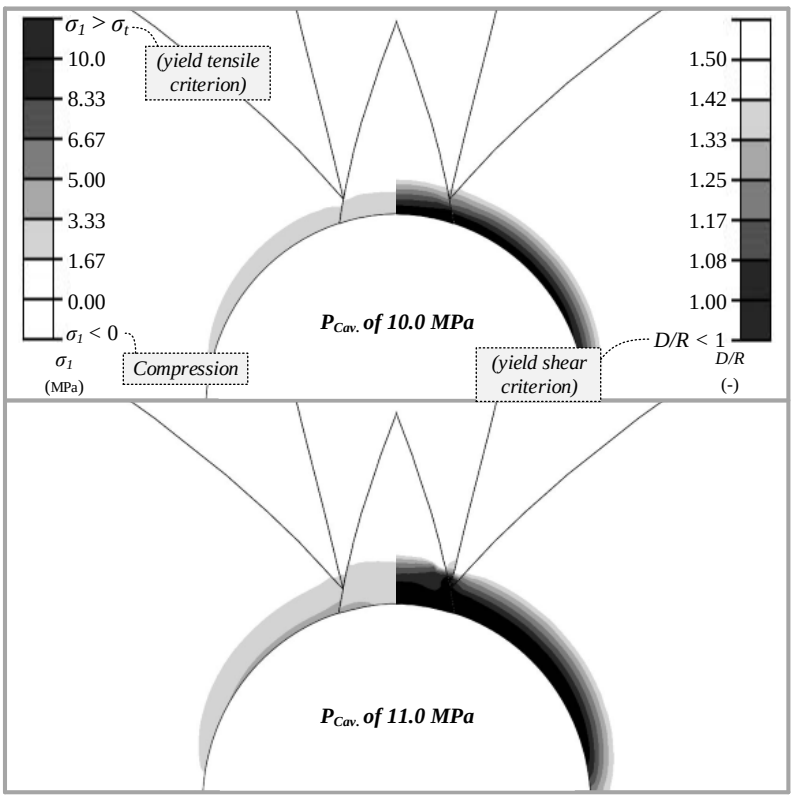

Figure 4.36 Shear fracture propagation

In the Figure 4.36, shear fracture propagation is also continuing along the shear failure path with increasing of the cavern pressure. Following conclusion can be drawn;

1. Continue propagating with shear fracture
2. Zones of D/R approaching 1 in rock mass along the cavern wall can be seen. This implies that many cracks with shear mode would initiate.
3. Need more advanced approach to investigate the complicated shear fracture behaviors

Moreover, in each propagation step considered, there are two possible shear failure planes. The difference of those planes in this study is defined by an inclination angles against the major principal plane (plane of σ_1). The first possible shear plane has an angle counterclockwise to the plane of σ_1 as shown in Figure 4.37 a), therefore the predicted shear failure path of this shear plane is a curve moving toward the vertical symmetry axis. In contrast, the other shear plane is defined by the angle clockwise to the plane of σ_1 as shown in Figure 4.37 b). Consequently, the failure path prediction by this shear plane has a curvature toward lateral side.

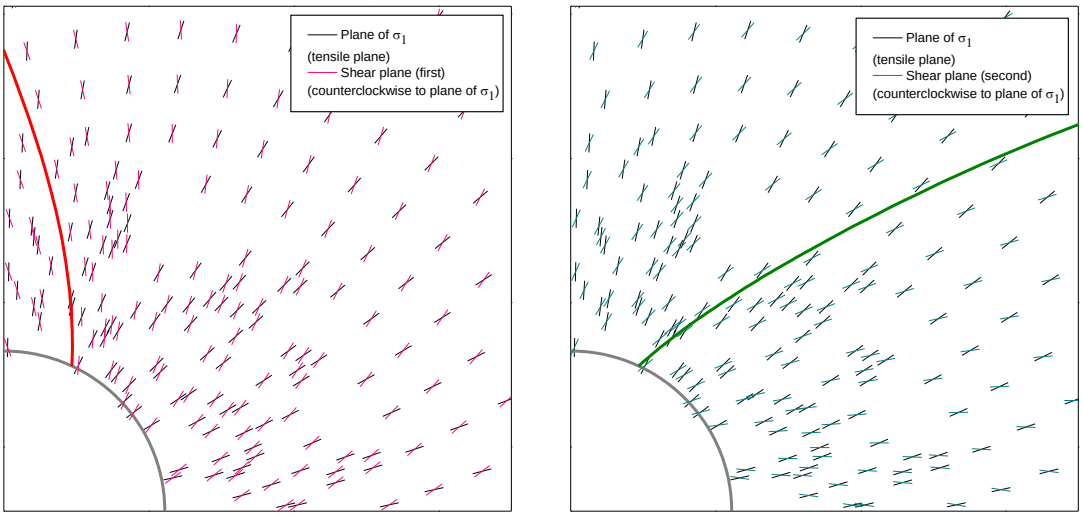

a) first shear plane (counterclockwise) and predicted shear failure path

b) second shear plane (clockwise) and predicted shear failure path

Figure 4.37 Defined shear planes and different predicted shear failure paths

Since there are two shear planes to be considered, the transition between shear planes is also investigated. From the continuing results of progressive failure analysis for shear fracture, herein shear fracture initially propagates along the first shear plane which counterclockwise against plane of σ_1 and then it does not change to the second shear plane which clockwise against plane of σ_1. From these results, it is concluded that the transition between shear planes is not occurred.

2. The change of failure path orientation

The progressive failure analysis in this section is to observe the change of failure path direction and then to evaluate the final potential failure path for both tensile and shear fracture. The change of failure path direction during crack growing is well-known in fracture propagation problem which resulted from the effect of stress redistribution. Besides, from the investigation in previous section, the effect of stress redistribution on the transition of failure modes was studied. Those results were concluded with three situations. First, based on the line of D/R=1, when a pair of C and σ_t locates above this line the fracture initiates with tensile mode and then it will prolong propagating with tensile fracture. Second, in contrast, with a pair of C and σ_t situated under the line of D/R=1, of which an initial crack starts with shear mode. The fracture can propagate under either shear or tensile mode if the relationship between σ_t and C is close to the line of D/R=1 because σ_t is not high enough to suppress the tensile fracture. Third, in case of σ_t is high enough for suppression the tensile fracture, only shear fracture can be seen. This situation is found when the relationship between σ_t and C are located far from the line of D/R=1.

To achieve the goal in this section which is to evaluate the final failure path for tensile and shear modes, the progressive failure analysis is performed separately by considering with tensile or shear failure. For tensile fracture, only tensile failure plane (plane of σ_1) is used to calculate a tensile failure path and then its pattern is prepared in a new FE mesh for the reanalysis. For shear fracture, it was investigated that the shear failure

plane obtaining a shear failure path that is close to the axis direction (shear plane which the direction is counterclockwise against plane of σ_1) is governed in shear fracture behavior. Therefore, only this shear plane is considered for the analyses in this section. The systematic progressive failure analysis in this section for evaluating the final tensile and shear failure path can be illustrated in Figure 4.38

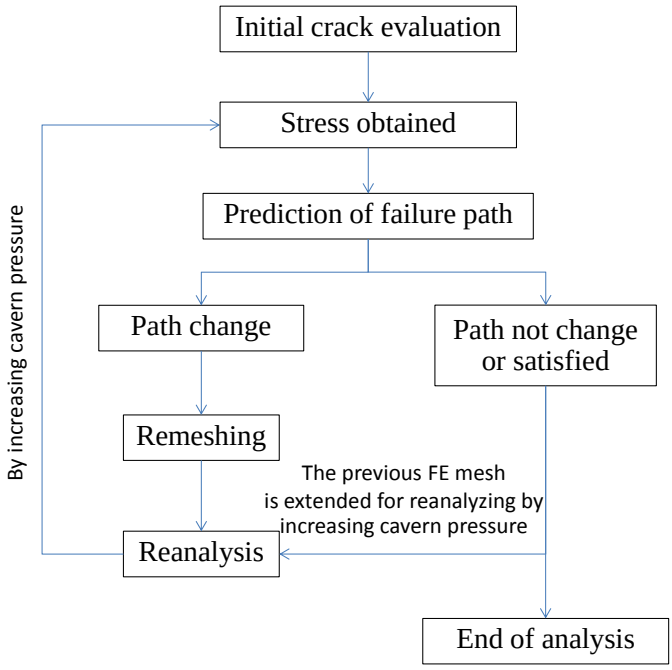

Figure 4.38 Systematic progressive failure analysis for evaluating the change of failure path direction considering the effect of stress redistribution

By using this systematic evaluation, final failure paths for tensile and shear fractures can be obtained. In the analyses of the change of failure path direction behaviors is due to the effect of stress redistribution, which in turn, relates to the change of principal plane direction. Figure 4.39 illustrates an example of the first cycle of the analyses by using this systematic evaluation for tensile fracture when k= 1, σ_t of 15 MPa and cavern depth of 60 meters (parameters in case 3). It indicates the change of the failure path behavior while the crack is propagating. This figure also shows the change of principal planes by comparing principal plane between at the initial crack state and at after crack propagation state. The principal planes at initial crack and after crack propagation are referred with cavern pressure of 33 (grey) and 35 (black) MPa, respectively. The figure indicates the different principal planes as illustrated by the trajectories of principal stresses. From this figure, it is seen that the trajectories of principal stresses after crack propagation state tend to shift to horizontal direction. Thus, the change of predicted failure path direction after partial crack has also a tendency with horizontal direction as well.

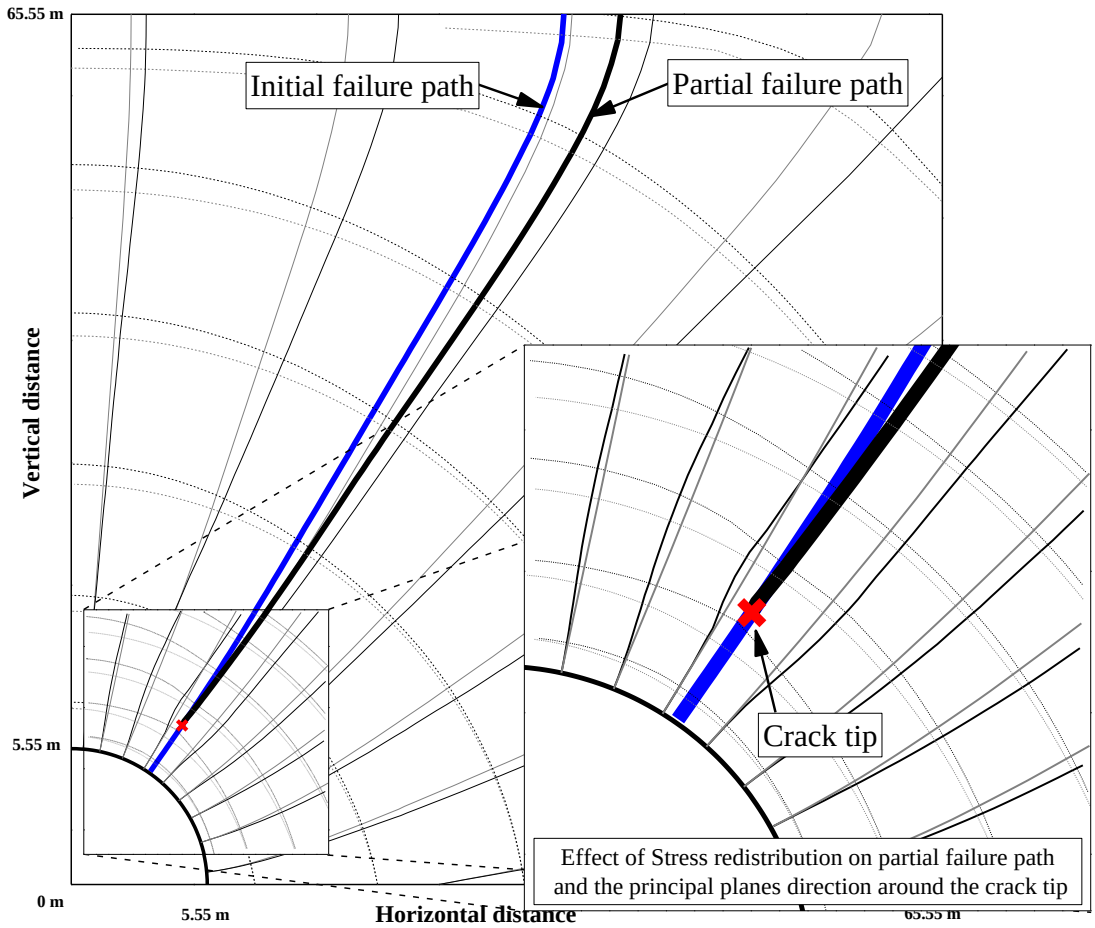

Figure 4.39 Effect of stress redistribution on the predicted failure path and the change of principal planes (tensile fracture)

The progressive failure analysis with adjusting the predicted failure path during increasing the cavern pressure was extended by repeating the mentioned process. In the analyses, the adjusted failure path is developed starting with the cavern pressure of 33 MPa, and, in turn, the stress state is reevaluated to adjust the failure path until the satisfied step (at 50 MPa). From this figure, it is seen that the partial tensile failure paths gradually moves to horizontal direction as shown in Figure 4.40. In the reality, with increasing of the cavern pressure and beyond the satisfied step of these analyses, the change of failure path direction will probably moves more horizontal direction.

In addition, the trajectories of principal stresses between two situations which are the stress state at initial crack induced by cavern pressure of 33(grey) and the stress state at satisfied step induced by cavern pressure of 50 (black) MPa are together plotted in order to illustrate the changes of principal planes between these situations which are the initial step and the satisfied step.

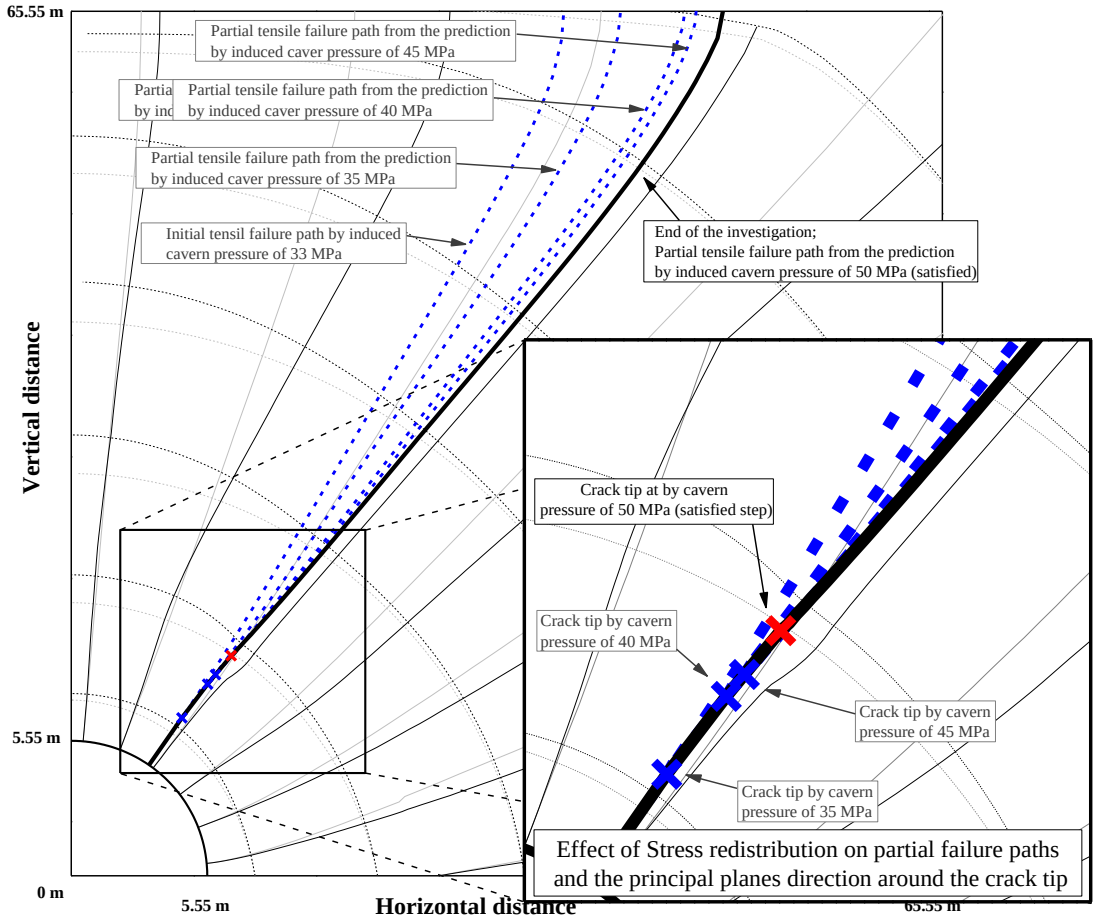

Figure 4.40 The influence of stress redistribution on evolution of predicted failure paths for tensile fracture case with σ_t of 15 MPa, k of 1 and cavern depth of 60 meters (parameter in analysis case 3)

Furthermore, by using the systematic evaluation, Figure 4.41 illustrates the adjusted failure paths for shear fracture when k= 1, C of 24.9 MPa and cavern depth of 60 meters (parameters in case 6). Developments of the adjusted shear failure paths can be seen. It starts with the cavern pressure of 33 MPa, and consequently, the stress state is reevaluated to adjust the failure path until the satisfied step (at 80 MPa).

Noted that, many certain levels of cavern pressure were performed to investigate the change of failure path in the analysis. Considering the failure path direction, it was found that the failure paths at many cavern pressures (after crack initiation at 33 MPa) were not changed until the level of cavern pressure reaches 70 MPa. Therefore, the reanalysis by remeshing in this case is then carried out with cavern pressure of 70 MPa. Figure 4.41 shows the partial failure path which is predicted by cavern pressure of 70 MPa. In this figure, the principal planes at initial crack and after crack propagation referred with cavern pressure of 33 (grey) and 70 (black) MPa. It is seen that the trajectories of principal stresses after crack propagation state tend to shift to horizontal direction which are also similar to cases under tensile fracture.

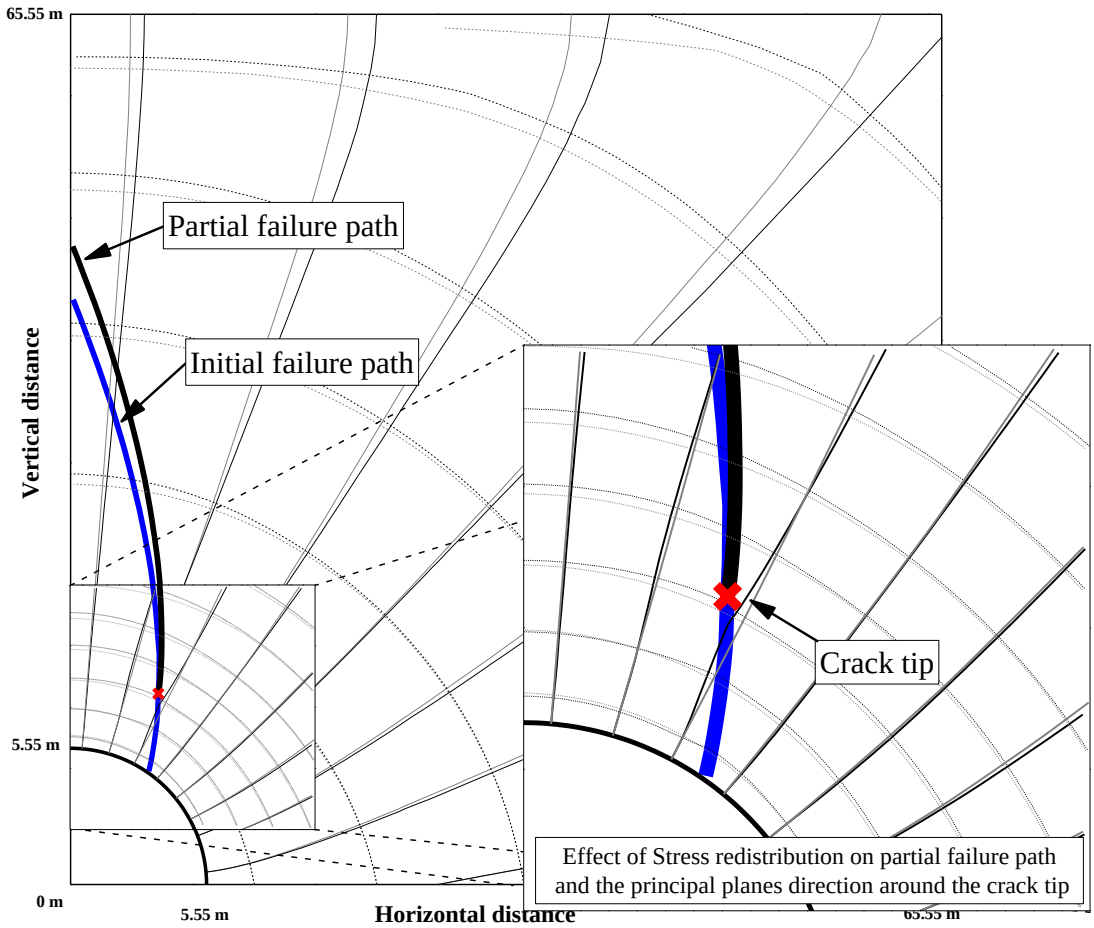

Figure 4.41 Effect of stress redistribution on the predicted failure path and the change of principal planes (shear fracture)

As a result, the analyses were performed until the satisfied step at cavern pressure of 80 MPa. It is seen that the partial shear failure path gradually adjusts and moves to vertical direction as shown in Figure 4.42. In the reality, with increasing of the cavern pressure and beyond the satisfied step of these shear analysis case, the change of failure path direction is expected to move vertically straight direction up to ground surface.

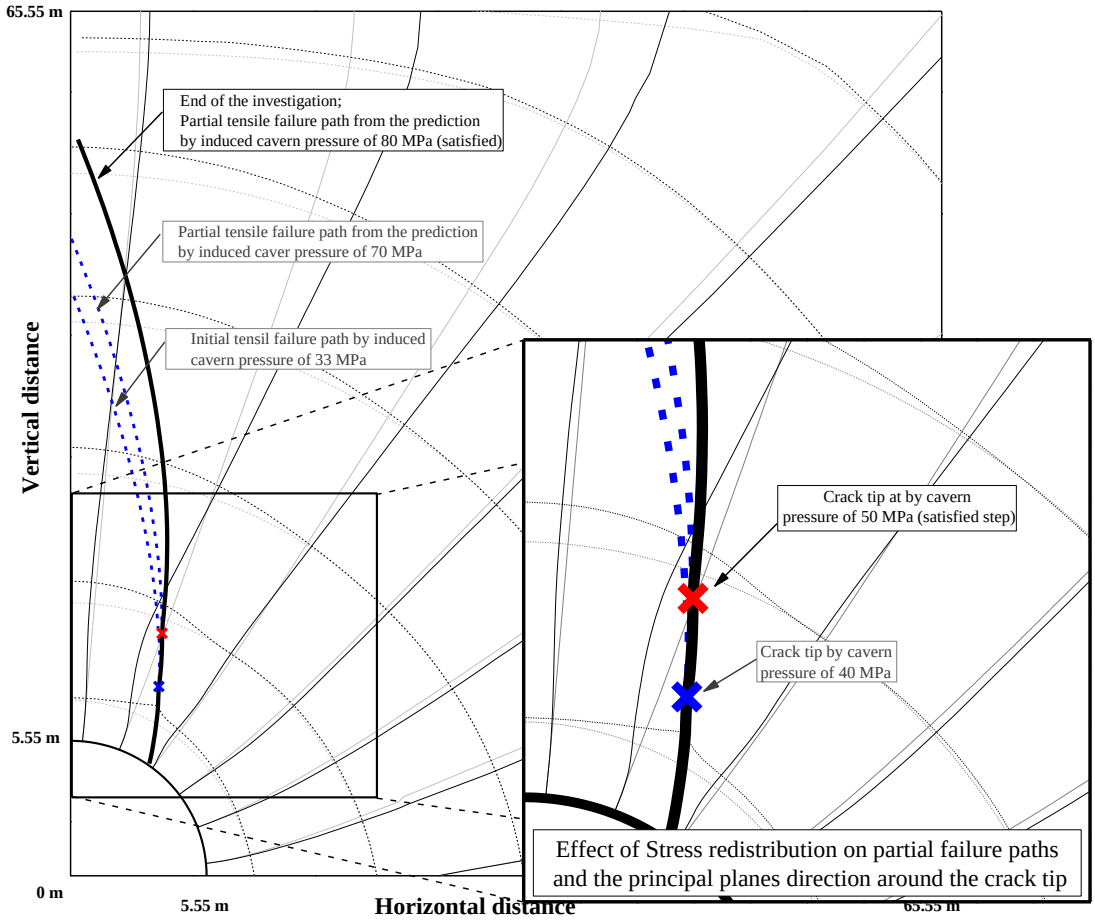

Figure 4.42 The influence of stress redistribution on evolution of predicted failure paths for tensile fracture case with *C* of 24.9 MPa, *k* of 1 and cavern depth of 60 meters (parameter in analysis case 6)

Based on the results of the change of failure path behaviors discussed for both cases, a simple tensile and shear failure path can be established. For tensile fracture, in spite of the fact that the fracture propagation will gradually moves more horizontal direction and its characteristic tends to be similar to the log spiral model (Ghaly and Hanna, 1994; see in Figure 2.4). However, a curvature of the log spiral model would be encountered with defining its curve.

In addition, as mentioned in preliminary evaluation on failure patterns in section 4.3, the *k* has influence on initial failure path (direction and degree of curvature). A further study considering the curvature for various *k* conditions is needed to understand the failure path change with various *k* conditions.

Thus, in this study, the simplest characteristic for tensile failure path is proposed (for every *k* conditions) as shown in Figure 4.42. This proposed tensile failure path is perpendicular to the cavern wall in radial direction. In contrast, the direction of shear fracture propagation can be simplified as a vertical straight failure path up to ground surface as shown in Figure 4.44. This shear characteristic is similar to the straight failure plane model proposed by JapanGasAssociation, 2008 (see in Figure 2.5). In

practical point of view, both tensile and shear characteristics which are proposed from this study are reasonable and conservative for evaluating the stability against ground uplift by using limit equilibrium method.

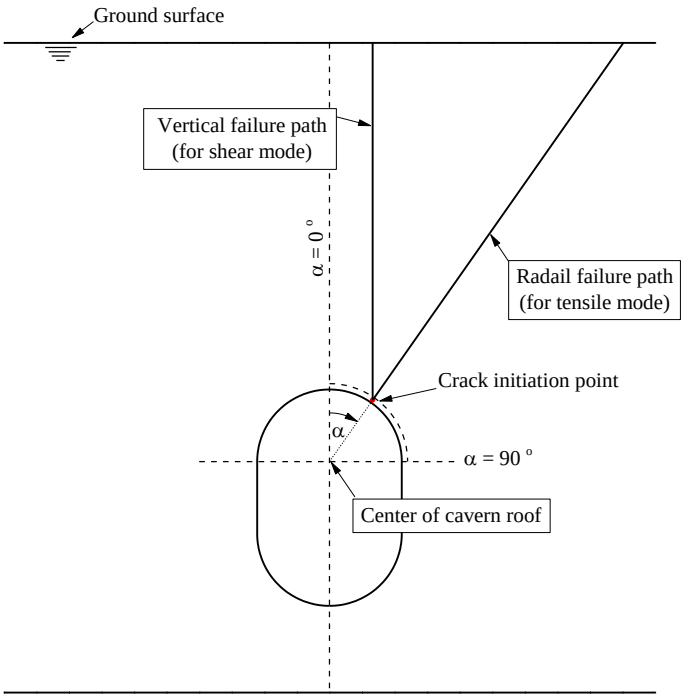

Figure 4.43 The proposed simple tensile and shear failure path

4.4.4 Verification case with previous study (Tunsakul et al., 2013)

According to Tunsakul et al. (2013) research (section 2.5.3), the pressurized cavern problem was conducted comparatively between the FEM interface-contact interaction and physical model tests. Those results were together redrawn and plotted so as to compare the results in each cases. The comparisons of the experiments were in good agreement with FEM with considered tensile mode in all cases as shown in Figure 4.45.

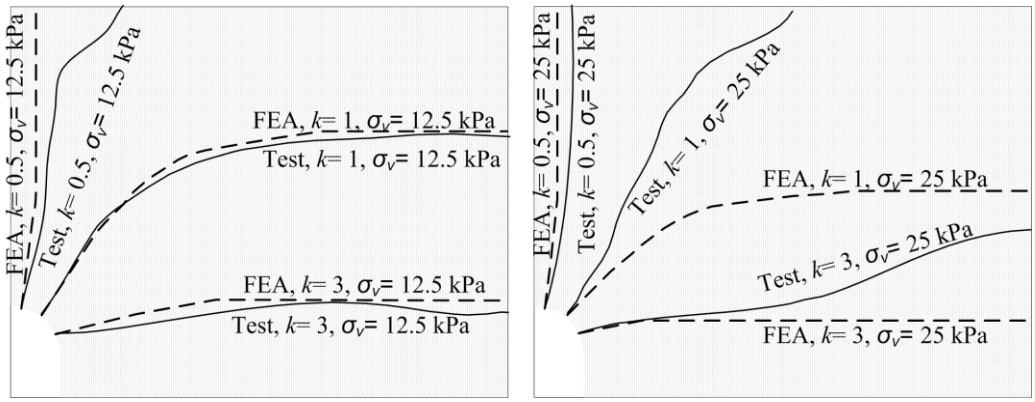

Figure 4.44 Comparison of FEM and Experiment test (Tunsakul et al., 2013)

As mentioned in this study, to support that the line of D/R=1 can be used to identify whether which fracture failure would propagate, thus, the artificial rock strength in Tunsakul et al. (2013) research especially σ_t and C are re-considered. The average

artificial properties of σ_t and C obtained by indirect tensile and direct shear testing are of 2.6 and 11 MPa respectively. It is noted that σ_t of 2.6 and C of 11 MPa are obtained by multiplying 200 which is the scale factor of those physical model test. This relationship is plotted in D/R chart appearing that locating on above the line of D/R=1 as shown in Figure 4.46. Thus, this issue indicates that tensile fracture is to be occurred for consideration in the line of D/R=1 concept.

Therefore, this mention has a strong support to the line of D/R=1 concept that it can be used to indicate which whether failure mode would be occurred considering in the wider range of rock strength properties.

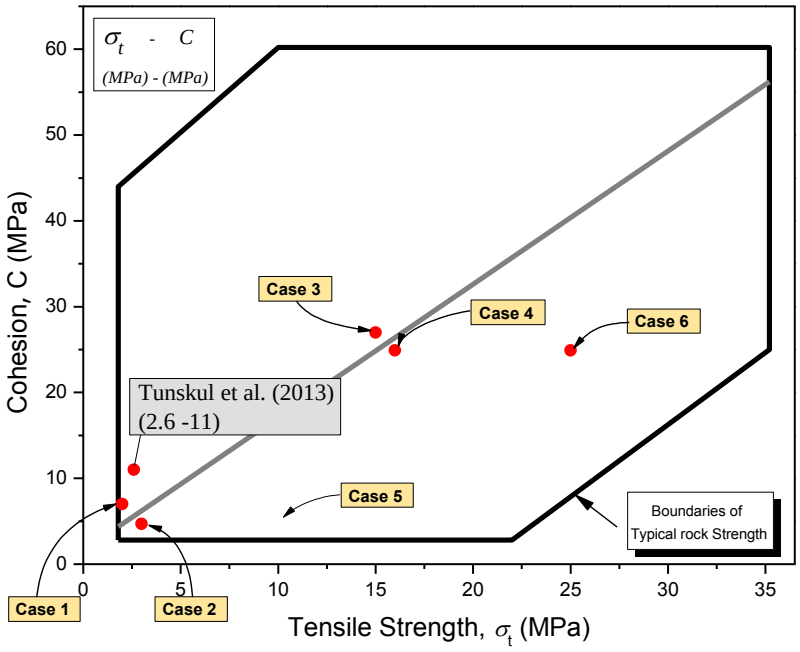

Figure 4.45 Fracture behaviors considered on pair of σ_t – C with the line of D/R=1

4.4.5 Conclusion

As the results of progressive failure analysis discussed above, it is concluded that tensile and shear fracture propagation can be occurred under applied cavern pressure depending on the rock strength properties. There are three situations to be accounted for. Based on the line of D/R=1, when a pair of C and σ_t locates above this line the fracture initiates with tensile mode and then it will prolong propagating with tensile fracture. In contrast, with a pair of C and σ_t situated under the line of D/R=1, of which an initial crack starts with shear mode. The fracture can propagate under either shear or tensile mode if the relationship between σ_t and C is close to the line of D/R=1 because σ_t not high enough to suppress the tensile fracture. Thus, in case of σ_t high enough for suppression the tensile fracture, the shear fracture can be seen. This situation is found when the relationship between σ_t and C are located far from the line of D/R=1.

In addition, a new crack location would be occurred with similar to its situation of the previous fracture behaving as described above (only tensile, either shear or tensile and only shear mode)

4.5 Established a simple chart for specifying initial crack location

From the analysis results in section 4.2, the initial crack location behaviors considering the possible rock strengths, cavern depths and *k* were discussed. Since, there were too many figures (see in section 4.2) used to elaborate the initial crack location behaviors. For this reason, in order to represent all results of initial crack evaluation with a simple chart and easy to use for specifying initial crack location, a relation of three factors is found by normalizing the rock strengths to the vertical stress representing the cavern depth values. Figure 4.47 shows the comparison between before and after normalizing rock strength by the vertical stress. All data obtained from the evaluation of crack initiation section (see in section 4.2) are plotted in a space of rock strengths (σ_t and C) against possible failure angle (α) for all *k* values and all values of cavern depth before the normalization Figure 4.47 a). A scattering of data for each *k* values can be seen. After normalizing rock strength by the vertical stress, the data have a good agreement for each *k* values as shown in Figure 4.47 b). Thus, to represent all data obtained, the relation of three factors could be found. Furthermore, by compromising and adjusting this good agreement data, then it is been re-plotted as solid lines for each *k* values in the space of failure angle - rock strengths as shown in Figure 4.47 b).

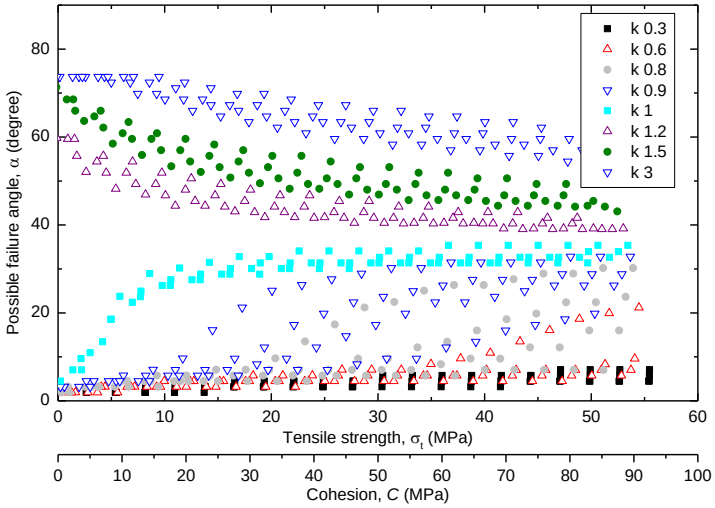

a) All data obtained from evaluation of crack initiation

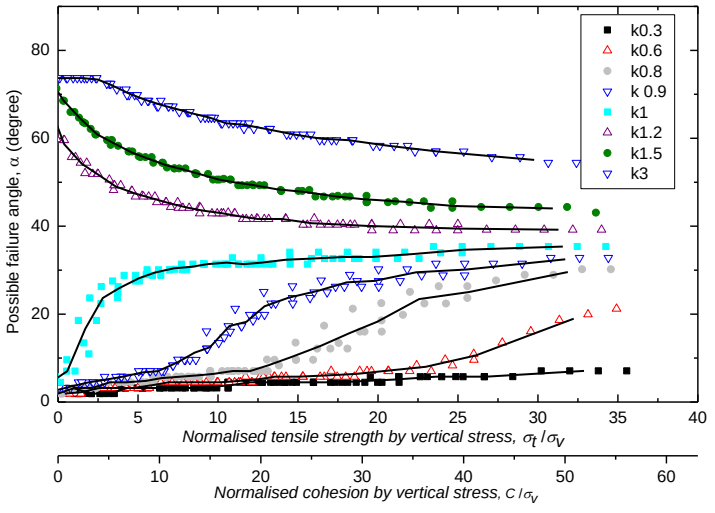

b) Normalized all data by vertical stress

Figure 4.46 The relation of three factors normalizing rock strength by vertical stress

Consequently, a simple chart to specify the possible failure angle is established as shown in Figure 4.48. The chart is from normalized all data by vertical stress as well as considering the wide range of rock strengths, cavern depth and *k*. The chart depicts the possible failure angle on the plane of *k* and normalized rock strengths with vertical stress. It is noted that there are two rock strengths (σ_t on left y axis and *C* on right y axis). The strength value to be used is that of the mode which reaches the failure criterion first.

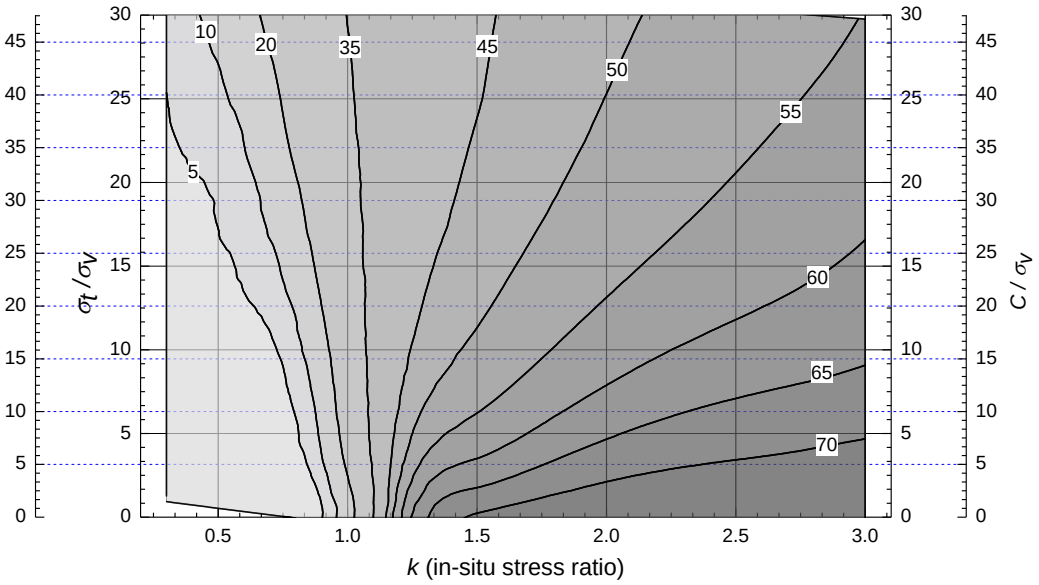

Figure 4.47 Chart for specifying initial crack location